29th Satellite Design Contest Satellite Overview

Application category
   Design Section
1. Work information/Applicants information

Work title (less than 20 words) MORSE (Moon Orbital Relay for South-polar Exploration)		
	Name	Affiliation including faculty, department (Lab) and year of study
Group representative	Vinícius Nery	Department of Aeronautics and Astronautics (Intelligent Space Systems Lab), 1st year Masters, Graduate School of Engineering, The University of Tokyo
Group representative (Sub)	Chang-Chin Wang	Department of Earth and Planetary Science (Usui Lab), 1st year Masters, Graduate School of Science, The University of Tokyo
Member 1	Adam Martin	School of Electrical, Computer and Telecommunications Engineering, 6th year undergraduate, University of Wollongong, Australia
Member 2	Matthew Chong	School of Engineering & IT, 3rd year PT Masters University of New South Wales Canberra
Member 3	Loïc Chalamet	Department of Materials Engineering (Pr Shibuta Lab), 1st year Masters, Graduate School of Engineering, The University of Tokyo
Member 4	Greeshma Shetty	School of Electrical Engineering and Telecommunications, 2nd year Masters, University of New South Wales

2. Outline of the satellite (approx. 200 words)

MORSE is a constellation of three microsatellites which will act as a commercial communications relay and provide positioning services to landers and rovers exploring the Lunar South Pole region. The three satellites will be placed in a highly inclined, elliptical frozen orbit around the Moon 120 deg apart from one another to achieve close to continuous coverage of the Lunar South Pole region with at least two satellites at a given time, to enable uninterrupted communications relay and positioning services.

3. Mission requirement (Aims of satellite) and significance

(a) Mission requirement (Aims of satellite)
The MORSE constellation aims to provide a continuous relay and positioning service to landers and rovers on the Lunar South Pole region. To achieve this it is necessary for at least two satellites to be in the field of view (FoV) of the rovers at all times and that at least one of the satellites is also in the FoV of the Earth's ground stations.

(b) Importance, technical significance
The Lunar South Pole region is the focus of many planned exploration missions in the coming decade. The presence of almost-eternal light makes it suitable for long-term lunar bases, and permanently shadowed regions (PSRs) may contain water ice and other volatiles. These areas are both located close to the scientifically interesting South Pole-Aitken Basin, which records the early history of the Moon and the rest of the Solar System. However, the lack of lighting in PSRs and limited line-of-sight for communication with the Earth are major challenges for landers and rovers exploring the Lunar South Pole region. MORSE will provide a means of overcoming those challenges.
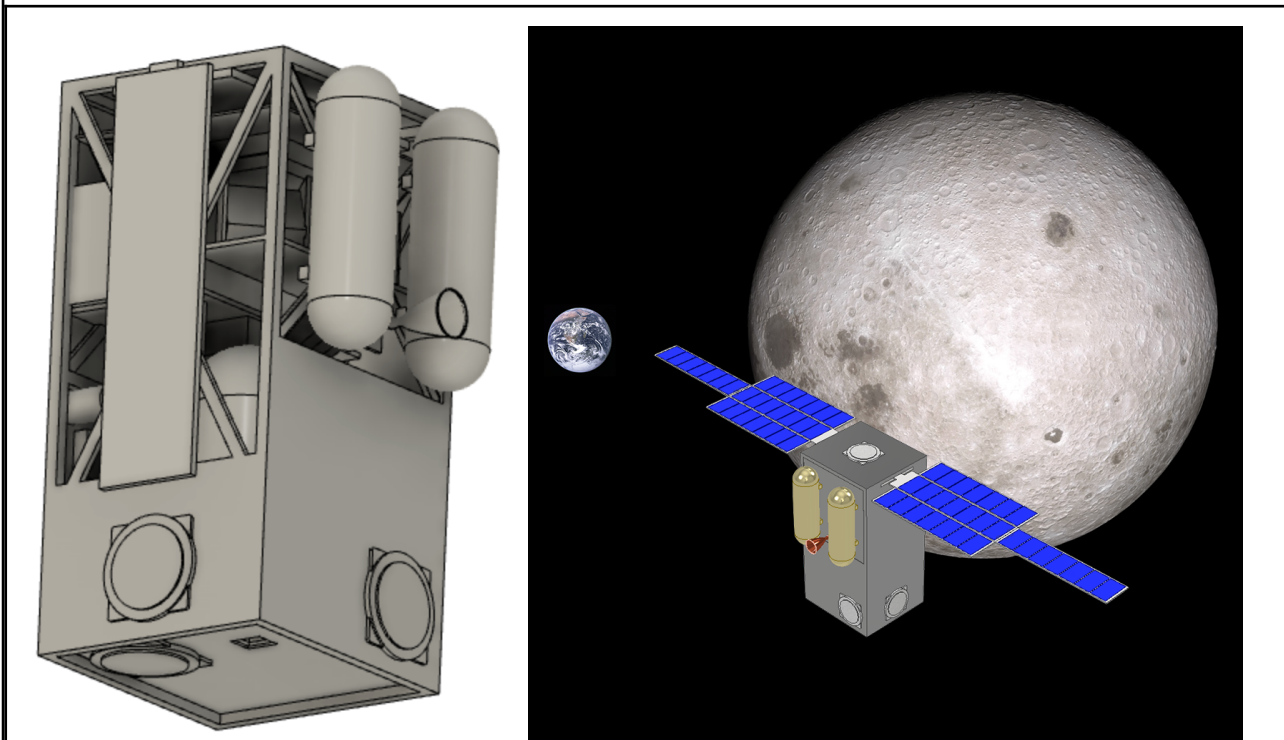
4. Anticipated results

The communication relay service is anticipated to provide continuous communication to rovers in the South Pole region of the Moon. The communication link is anticipated to achieve 1 Mbits/s or greater. The positioning service is anticipated to provide a low level of accuracy as the technology and deployment have low technology readiness levels. The mission is intended to be a proof of concept and potentially generate some level of revenue from the communication relay and positioning service.

5. Originality and/or social effects

While the idea of a lunar constellation relay to assist lunar exploration is not original by itself, the means to achieve the relay proposed by the MORSE mission are indeed original. First, considering advancements in space technology, we propose a three-microsatellite constellation to set up the relay system at a low cost. Furthermore, a theoretically studied frozen orbit configuration will be used, which can provide valuable data for future Moon missions that seek to maintain constellations of satellites without much station-keeping. Moreover, a two-satellite positioning system as an initial step to a Lunar Navigation Satellite System (LNSS) will be tested. Therefore, the proposed relay and positioning systems can greatly benefit future Lunar exploration missions.

6. Result of satellite design

(a) System (overall configuration, shape, mass, function, operational orbit)

Dimensions	212.5 x 441.25 x 238.2 mm^3	**Wet Mass (per spacecraft)**	15492 g
Orbit	881 x 8730 km, 56.2^0 frozen Lunar orbit with three satellites positioned 120^0 apart in terms of mean anomaly	**Payload/ TT&C**	- S-band patch antenna (x6) - Transceiver (x2) - Coaxial cable (x2) - Chip-scale atomic clock
Propulsion	10 N bipropellant main thruster - Custom propellant tanks and xenon pressurization tanks	**ADCS**	- Star Tracker - Sun Sensors (x2) - IMU - Reaction Wheels (x4) - Cold Gas RCS Thrusters (x4)
Structure	- Aluminium 7075-T6 - First-order natural frequency: 253.6 Hz	**Thermal Control**	12 W heaters (x10) - Hottest temperature : 37°C

	● Mass : 4.1 kg		● Coldest temperature : -9°C ● Anodized aluminium structure ● S13G-LO white paint on the back of the solar panels
Electrical Power	● Deployable sun-tracking solar array panels (total BOL power: 56 W) ● Modular EPS ● Battery arrays (x11, total capacity: 488.4 Wh)	**C&DH**	Onboard Computer

(b) Experimental system including ground stations
Four ground stations from Near Earth Network are selected to provide constant coverage of the satellites.
- KSAT Singapore — Assets: 9.1m
- South Point, Hawaii — Assets: 13m
- Santiago, Chile — Assets: 9m, 12m, 13m
- Hartebeesthoek, South Africa — Assets: 10m, 12m

(c) Operational procedure including data acquisition
The satellites will be delivered into a Lunar transfer trajectory by the launch vehicle. When they arrive at the perilune, the satellites will use their chemical thrusters to enter the mission orbit and position themselves 120° apart. In the mission orbit, the two satellites with line-of-sight with the Lunar South Pole at a given time will broadcast positioning signals, and at least one of them will relay data between clients on the Lunar surface and ground stations on Earth. When a satellite is out of line-of-sight with the Lunar South Pole, it will be in Safe Mode, occasionally transmitting telemetry and tracking signals to the ground station.

7. Concrete achievement methods, range and budget for manufacturing

The mission is developed with product readiness in mind. For space, ground, and launch segments, components are chosen from commercial-off-the-shelf (COTS) products or services. Furthermore, most COTS components have flight heritage which provides data to support their performance and technology readiness level (TRL) from previous missions. Using these components provides a higher likelihood of success.

Based on available cost figures of COTS hardware, a hardware budget of 1.5 million USD is estimated for the space segment (3 satellites). This does not include the ground segment (use of ground stations) and launch segment.

8. Development, manufacture and launch schedule

As there are three satellites in total, we consider an estimated time of about 9 months to obtain funding, develop all three satellites, and plan for procurement of necessary materials and items. Furthermore, from finding a manufacturer and planning logistics to pre-launch processing at the launch site will take approximately 15 months. The satellite is planned to launch in November 2023 aboard an H-IIA launch vehicle from the Tanegashima Space Center. This is such that the mission time aligns with the Lunar South Pole exploration projects, and to facilitate communication with landers and expectantly with astronauts on the far side of the moon.

MORSE: Moon Orbital Relay for South-Polar Exploration

1. Aims and Purposes

This decade will see an unprecedented expansion of Lunar exploration activities. NASA's Artemis Program aims to return astronauts to the Moon for the first time since the conclusion of the Apollo Program in the 1970s. Other major space-faring nations including China, Russia, and Japan are all preparing for robotic Lunar missions with the long-term aim of establishing crewed Lunar bases [1] [2] [3], and various smaller space agencies and private entities are also developing their own Lunar missions [4].

Many of the proposed missions are focused on the region around the Lunar South Pole, where several unique features make it valuable from both scientific and exploration perspectives. The low incident angle of sunlight creates permanently shadowed regions (PSRs), which are believed to contain deposits of cold-trapped volatiles such as water ice. Evidence of volatiles have been found by orbital remote sensing both in and out of PSRs around the Lunar South Pole [5], but the PSRs provide the most favorable thermal conditions for volatiles to exist [6]. These deposits contain information about the delivery of volatiles in the more recent part of the history of the Solar System. They are also a potential source of water, oxygen, and propellant through in-situ resource utilization [6].

In contrast, some peaks on crater rims in the region receive almost permanent illumination by sunlight, up to more than 80% of the time [7]. Compared to most other regions of the Moon where nighttime lasts for half a month, these peaks provide more reliable access to solar power and less extreme temperature variation, making them

suitable sites for long-term robotic missions and crewed bases for exploration [8].

The Lunar South Pole sits on the rim of the South Pole-Aitken Basin, a farside region of high scientific interest. The basin is the largest and oldest impact crater known in the Solar System, preserving records of its early history [5]. Clarification of its geological history of the basin can provide constraints to the evolution of the Moon and the rest of the Solar System, from how large impacts shaped the surface and interior of the Moon to the movement of gas giants that may have caused a period of violent impact events known as the Late Heavy Bombardment. Created by a giant impact that excavated deep subsurface materials, the basin is also a window into the composition of the lower crust and/or upper mantle of the Moon, which is still poorly understood [9]. The scientific importance of the South Pole-Aitken Basin makes the South Pole the focus of many upcoming missions compared to the North Pole [5].

The high latitude that created PSRs and peaks of near-eternal light also poses challenges to exploration. The lack of sunlight in PSRs means that conventional optics-based navigation methods for rovers such as visual simultaneous localization and mapping would not work [10]. Although the Moon is tidally locked to the Earth, due to the axial tilt of the Moon relative to its orbital plane, the Earth is only visible from the Lunar South Pole for 14 days and then sets below the horizon for another 14 days. Even when it is above the horizon, its low inclination (<=6.5deg above the horizon) coupled with the rugged terrain around the Lunar South Pole mean that continuous and direct communication with the Earth is

impossible from many places in the region [8]. As a result, lighting and communication considerations are expected to significantly limit where landers and rovers can explore near the Lunar South Pole [5], which would negatively affect the ability to gather data and resources.

MORSE, a constellation of relay and positioning satellites, aims to mitigate these problems and make exploration of the Lunar South Pole region easier, more productive, and more accessible. By relaying signals through satellites located high above the horizon, landers and rovers can maintain communication links even from the bottom of deep craters. A satellite-based positioning service can, similar to GPS on Earth, allow rovers operating in the darkness of PSRs to obtain their positions without relying on visual landmarks. The relay and positioning services will be offered commercially to all paying customers. Compared to dedicated relay satellites attached to specific missions, like the Queqiao satellite that supported the Chinese Chang'e 4 lander [11], MORSE will allow a wider range of clients to take advantage of its service, including smaller missions that would not be able to afford a dedicated support satellite.

2. Anticipated Results

The MORSE mission is expected to have a five-year operational lifetime. Over this period, it is anticipated that the satellites remain in their frozen orbit to provide services specified in Section 1. As most of the systems and products have been over-designed to exceed mission requirements in worst-case scenarios, the satellites could potentially operate beyond the five-year lifetime.

The communication data rate between Earth and MORSE satellites is expected to be 1 Mbps or greater, and that between the Lunar surface and MORSE satellites is expected to be 4 Mbps or greater. As the communication relay service focuses on the South Pole region of the Moon, it is anticipated that this service could support Lunar rovers from national or private organizations without limitation from political concerns.

The positioning aspect of this service is a proof of concept. The positioning accuracy is expected to be quite low, but it could be used in conjunction with a positioning beacon from a rover or lander to enhance the accuracy. The use of the communication system and the positioning system is a charged service, with generated revenue to be fed back into the mission for improvements. These improvements could include launching more satellites into the constellation for improved accuracy, precision, and redundancy.

3. Originality and Impact

The main aspect of the MORSE mission is acting as a relay for future Lunar South Pole exploration, an aspect which by itself does not bring along much originality considering that similar missions have been proposed by NASA (Lunar Relay Satellite Network) and the Chinese Lunar Exploration Program over the past few years. However, the originality of the MORSE mission lies in its means to achieve such a relay constellation. Considering the current advancements in space technology, a mainly commercial-off-the-shelf, three-microsatellite constellation is proposed to set up the relay system at a relatively low cost. Furthermore, a theoretically studied frozen orbit configuration

capable of maintaining stability for 10 years providing full coverage of the Lunar South Pole will be used. Data collected from this mission can therefore provide valuable information for future Lunar missions, especially for low-station-keeping satellite configurations.

The MORSE mission intends to establish a relay service which offers support to multiple users on the moon. This support includes a low spatial resolution positioning system as an initial step to a Lunar Navigation Satellite System (LNSS) that will be necessary in the future. The position data acquired aims to validate proposed algorithms and act as an asset for ongoing research. Considering these aspects of the MORSE mission, its value and potential benefits for future Lunar exploration missions are well defined.

4. Design Result

4.1. Orbital Analysis

MORSE is a constellation of three micro-satellites that will be placed in an elliptical frozen orbit around the Moon. The targeted area for our mission is the Lunar South Pole, with the mission orbit being selected based on [12]. The Keplerian elements that define the orbit of one of the satellites are summarized in Table 1. The semi-major axes for the other two satellites are within the same range but varied slightly to prevent secular drift of the relative mean anomaly over

time. The mean anomalies of the satellites in the orbit are adjusted to be 0º, 120º and 240º to have a close to continuous coverage of the Lunar South Pole. The orbit is a frozen orbit, which [12] proved to be stable for at least 10 years without the need for a rigorous deterministic control.

Table 1: Keplerian elements of the mission orbit

Semimajor Axis	6,541.4 km (Satellite M1)
Eccentricity	0.6
Inclination	56.2º
Argument of Perilune	90º

The mission was simulated in Systems Tool Kit (STK) to confirm the feasibility of the mission. The above orbital parameters were set and the HPOP propagator in STK was used, which took into consideration factors such as atmospheric drag and solar radiation pressure.

The Chandrayaan landing site (89.9ºS, 0ºE) was used in the simulation as the location of an example client in the Lunar South Pole region. Although the farside away from the South Pole is not the primary focus of the mission, the Chang'e 4 landing site (45.457ºS, 87.589ºW) was also included in the simulation, and the result showed good temporal coverage even in the southern mid-latitudes.
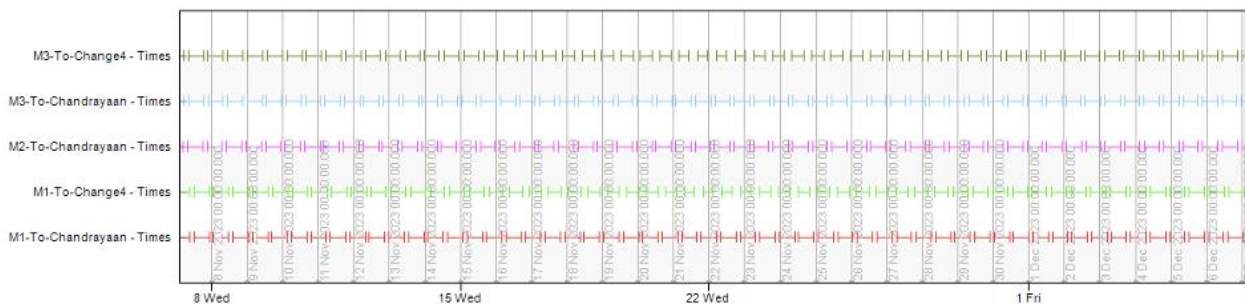

Figure 1: Coverage of the MORSE constellation at the landing sites of Chang'e 4 and Chandrayaan

Coverage of the South Pole is provided by at least 2 satellites at a given time and constant line of sight to Earth ground stations is achieved (Figure 2). For continuous access, 4 ground stations are considered: Singapore, South Point (Hawaii), Santiago (Chile), and Hartebeesthoek (South Africa) (Refer to Section 4.3 for the coordinates of the ground stations).
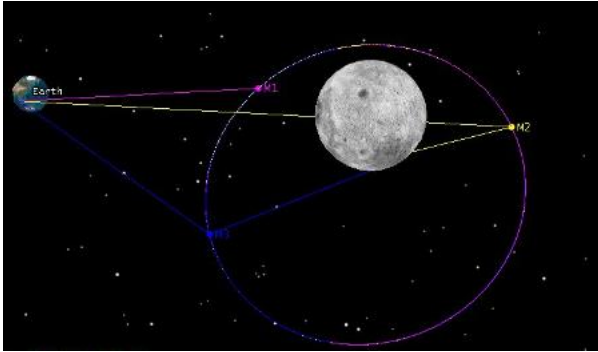

Figure 2: The mission orbit in STK showing LOS with a ground station on the Earth for all three satellites.

4.1.1 Launch and Orbital Transfer

The satellites will be launched onboard an H-IIA rocket to lift off from the Tanegashima Space Center in Japan. In order to strategically utilize the launch vehicle's ΔV budget, the satellites will be released from the launch vehicle once it reaches a Lunar-transfer trajectory. The magnitude of ΔV needed to perform the Lunar orbit insertion (LOI) maneuver is 345.9 m/s. The launch is planned for 1st November 2023 and intended to reach the target point for LOI by 7th November 2023. The Astrogator propagation model was used to study the path of the satellites. The transfer trajectory is hyperbolic in nature as shown in Figure 3.
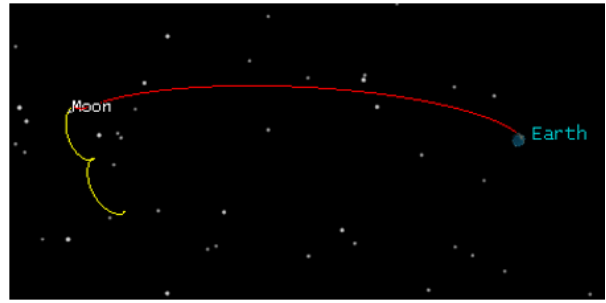

Figure 3: STK/Astrogator simulation of the transfer trajectory

4.1.2 Orbital Phasing

After entering the mission orbit close together, the three spacecraft need to be positioned such that their mean anomaly is offset by 120⁰ from one another to achieve continuous coverage of the Lunar South Pole with at least two satellites. The phasing maneuver will be conducted by slightly varying the semimajor axes of two of the satellites at perilune so that one has a shorter period and the other has a longer period than the third satellite, whose orbit will not be changed. Over time, the three spacecraft will drift apart. When the desired separation is achieved, the two spacecraft in altered orbits will fire their thrusters again to return to the original mission orbit. Figure 4 is a graphical explanation of the maneuver.

Six orbits are assumed to be a reasonable time to complete the phasing maneuver. To achieve 120⁰ of relative mean anomaly in six orbits, the difference in mean anomaly between a satellite in the adjusted orbit and one in the original orbit per adjusted orbit, ΔM_{a0}, should be:

$$\Delta M_{a0} = \frac{Desired\ relative\ mean\ anomaly}{Number\ of\ orbits}$$

$$= \frac{120°}{6\ orbits}$$

$$= \frac{20°}{orbit}$$

We define $|\Delta T| = |T - T'|$ as the magnitude of the difference between original (T) and adjusted orbital periods (T'). The relationship between $|\Delta T|$ and ΔM_{a0} can be expressed as:

$$\Delta M_{a0} = \frac{|\Delta T| \times 360°}{T} = \frac{20°}{orbit} \qquad (1)$$

Since T is already known to be 47,464 s, we can solve for $|\Delta T|$ = 23,732 / 9 s and T' = 44,827 s or 50,101 s. Then the semimajor axes of the two possible adjusted orbits, a', can be calculated as follows:

$$a' = \left[\frac{GMT'^2}{4\pi^2}\right]^{\frac{1}{3}} \qquad (2)$$

This gives 6,296,800 m or 6,781,500 m, where the semimajor axes calculated are the results of prograde and retrograde maneuvers at perilune.

The velocity at perilune after maneuvering, v'_{pe}, can be calculated by the vis viva equation:

$$v'_{pe} = \left[GM\left(\frac{2}{r_{pe}} - \frac{1}{a'}\right)\right]^{\frac{1}{2}} \qquad (3)$$

Where r_{pe}, the perilune radius, is 2,616,560 m, so we can obtain v'_{pe} = 1,723.4 m/s or 1,739.5 m/s.

The perilune velocity of the original mission orbit, v_{pe}, can also be calculated by the same equation as 1731.87 m/s. The magnitude of the ΔV for adjusting the orbit is:

$$|\Delta v| = |v_{pe}' - v_{pe}| \qquad (4)$$

Which results in 8.47 m/s or 7.63 m/s. If one satellite does an 8.47 m/s retrograde maneuver while another does a 7.63 m/s prograde maneuver at the perilune, both satellites will achieve 120⁰ of relative mean anomaly with each other and the third satellite remaining in the original orbit after six orbits. The time required to complete the phasing maneuver can be calculated by multiplying the longer orbital period of the two adjusted orbits by 6. This computation will reveal that the maneuver can be completed in 83.5 h.

After reaching 120⁰ of relative mean anomaly, the two satellites in adjusted orbits will need to perform another maneuver to return to the original mission orbit. The total ΔV required for the phasing maneuver is twice the amount required for the initial orbital adjustment, or 16.94 m/s and 15.26 m/s for the two satellites, respectively. With some safety margin included, each satellite will have 20 m/s of ΔV budget for the phasing maneuver.
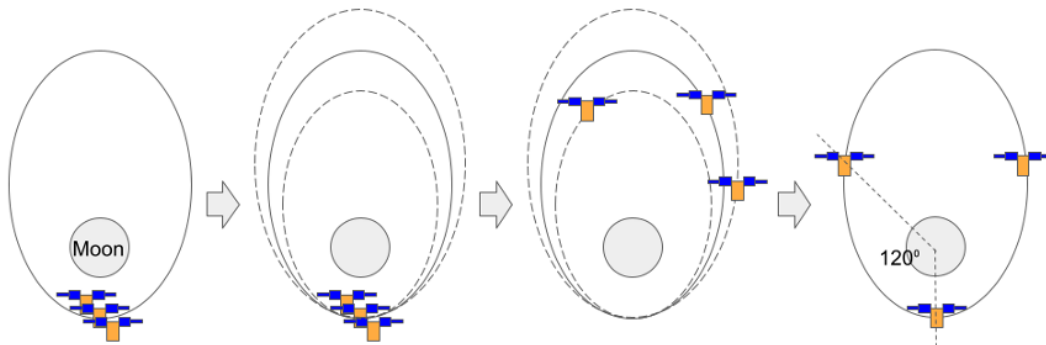

Figure 4: Orbital phasing maneuver

4.2. System Description

4.2.1. Structure and Mechanism Subsystem (SMS)

The progression logic for this subsystem is iterative. The first step was to create a metal frame that could withstand the various loads associated with launch, using Autodesk Inventor. Once these constraints had been met, the various components from other subsystems had to be placed, while ensuring compliance with not only the mechanical constraints imposed by the rocket but also the restrictions in terms of mass, available space, and mass distribution inside the satellite.

Table 2 : Random vibration (3 axis-common)

20~200Hz	+3db/oct	Effective value 7.8Grms
200~2000Hz	0.032G2/Hz	

Table 4: Sine wave vibration level

Axis direction	2.5 G	5~100Hz
Axis orthogonal direction	2.0 G	5~100Hz

4.2.1.2 Material Selection

The structure ensures the physical integrity of the components during launch and operation of the satellite. Therefore, a material with high tensile strength and low density is required. Aluminum 7075 T6 is the ideal candidate to meet these conditions. It is a material commonly used in aeronautics and its useful mechanical properties are summarized in Table 6.

Table 6: Mechanical properties of aluminum 7075 T6

Density	2.81 g/cm3
Young Modulus	71.7 GPa
Poisson's ratio	0.33
Tensile Yield Strength	503 MPa

4.2.1.1 Constraints from Launch Environment

The major mechanical stresses on the satellite come from the launch phase, during which the structure is subjected to high loads. The launch environment is derived from the characteristics of an H-IIA rocket, whose properties are described in Tables 2-5. The maximum mass allowance is 50 kg. Since we are using a constellation of 3 satellites, each one should not exceed 16.6 kg. In addition, the satellites must be contained in a cube 50 cm wide. Size and mass are therefore key factors for the success of the project.

Table 3 : Quasi-static acceleration

Axis direction	+5.0/-6.0G
Axis orthogonal direction	±5.0G

Table 5: Rigidity requirement

Thrust direction	higher than 120Hz
Lateral direction	higher than 60Hz

4.2.1.3 Modal Analysis

The finite element software ANSYS is used to perform the mechanical calculations. The first step is to check that the frequency of the first mode of vibration when the base is integrated with the launch vehicle is higher than required. This is to avoid resonance, which would have dramatic consequences for the success of our mission. The first 10 modes are calculated so that the cumulative effective mass is sufficient not to miss a significant deformation mode. To stiffen the structure without consuming too many precious kilograms, diagonal braces are used as can be seen in Figure 5.
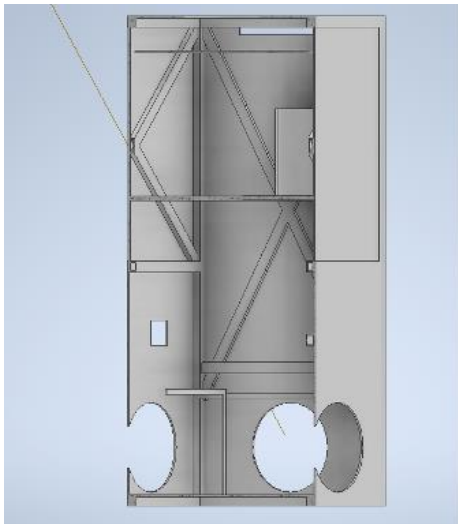
Figure 5: Sectional view of the structure alone

To clearly show the location of the deformation, we choose to hide the components other than the structure when presenting the deformation of the first 10 modes. All components were given the same elastic properties as aluminum.

The constraint related to the rigidity of the structure is met since the frequency of the first mode is higher than that required. The first mode in the thrust direction is 253.6 Hz, which is greater than the 120 Hz required. The first mode in the orthogonal thrust direction is at 264.5 Hz, which is also higher than the requirement of 60 Hz.

4.2.1.4 Random Vibration Analysis

The purpose of this analysis is to determine the response of the structure to random loading representing possible shocks during launch. The result of the simulation is shown in Figure 7, displaying the equivalent stress in MPa with a confidence interval of 3σ.

The first remark that can be made is that the maximum stress is about 120 MPa. As a reminder, the tensile yield strength is 503 MPa. The deformation therefore remains purely elastic. The safety factor is then $n = \frac{503}{119.24} = 4.22$ which is greater than 1. If we look more precisely at the result, particularly at the distribution of stresses, we notice that these correspond to the response of the structure to the main deformation modes.
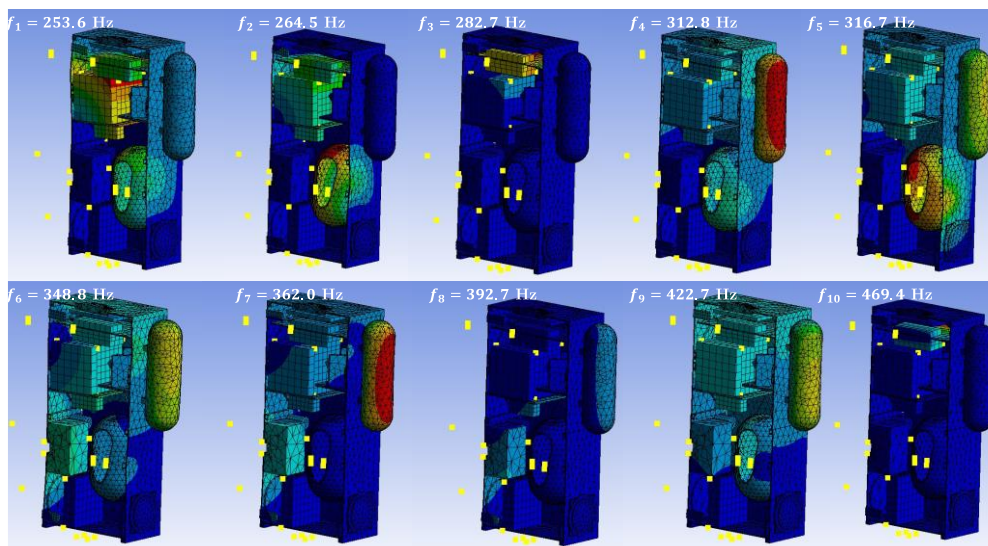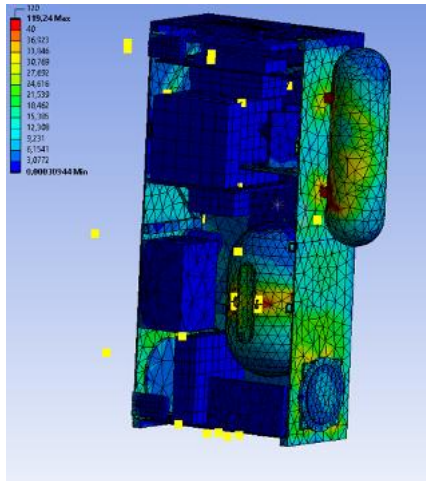

Figure 6: Deformation of the first 10 modes

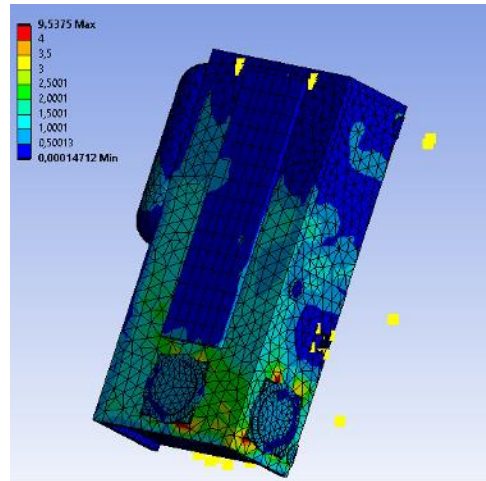**Figure 7: Equivalent stress in random vibration analysis**

Figure 8: Equivalent Von mises stresses put in the case -6G in axis direction /-5G in orthogonal direction.

4.2.1.5 Quasi-Static Analysis

A quasi-static analysis is then performed to calculate the forces in the structure subjected to acceleration during launch. The equivalent stress of von Mises in MPa is shown in Figure 8. Here again, the maximum stress is 9.54 MPa. The safety factor is then $n = \frac{503}{9.54} = 52.7$, which allows us to conclude that the structure can resist the acceleration of the launch phase.

4.2.1.6 Sine Wave Vibration Analysis

The sine wave analysis is intended to represent low-frequency launch conditions. The test frequency range is 5 Hz to 100 Hz. The imposed stiffness constraint is found here. Indeed, if the fundamental frequency is lower than 100 Hz, resonance would occur.
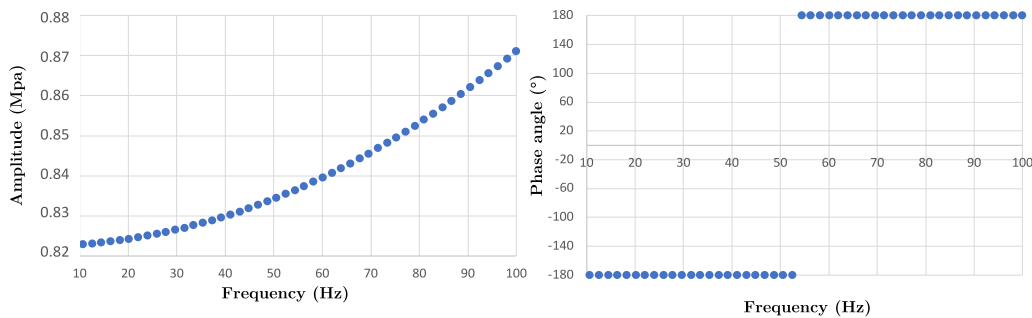

Figure 9: Evolution of the maximum shear stress as a function of frequency

4.2.1.7 Assembly of the Various Components in the Spacecraft

In order to get a better idea of the internal layout of the different components Figure 10 shows the model without the structure.

4.2.1.8 Coordinates of the Spacecraft's Faces

To easily distinguish the different faces of the satellite, we propose to name each face according to the normal vector to the face. Figure 11 shows the orthonormal coordinate system used and some faces of the satellite.

4.2.2. Thermal Control Subsystem (TCS)

The temperature range to which the satellite is subjected is significant. There are situations in which the satellite receives a large heat flux when it is oriented towards the sun or
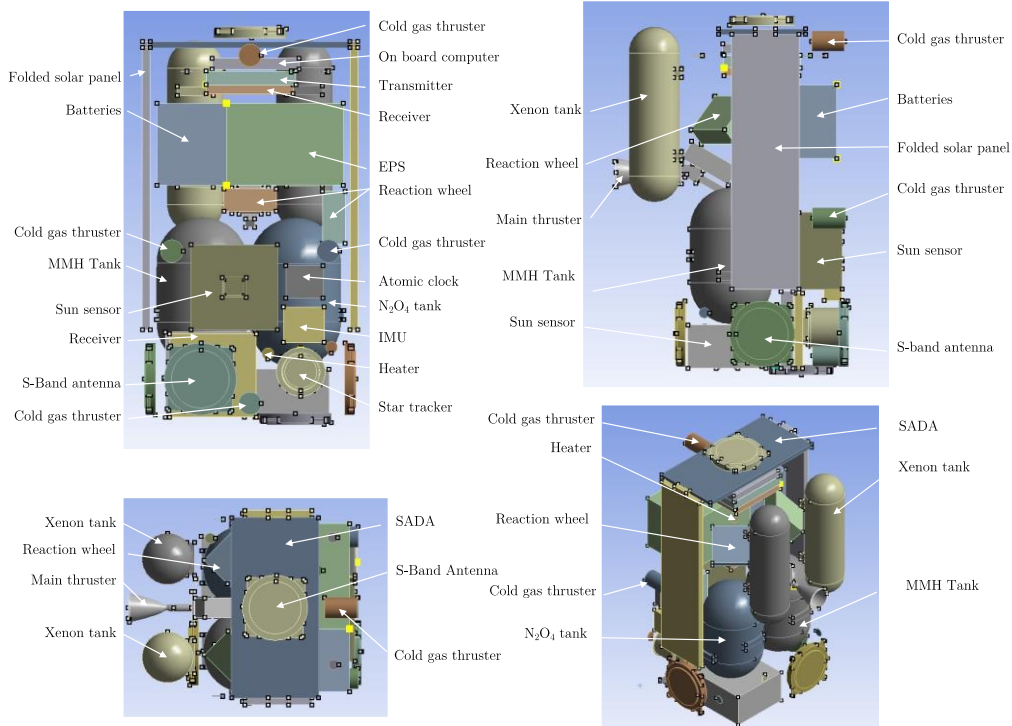
Figure 10: Assembly of the different components inside the spacecraft
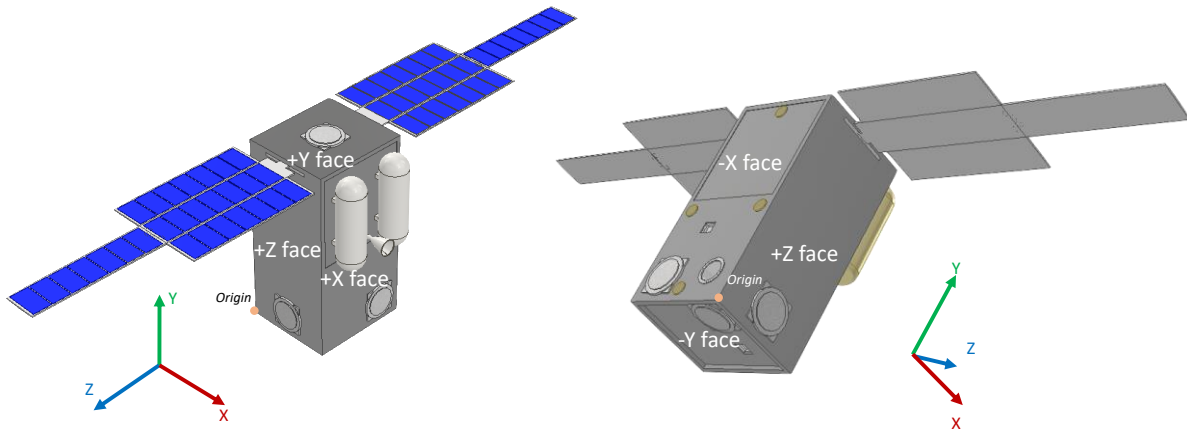
Figure 11: Coordinate system

very little when it is in the shadow of the Moon or Earth. Since components have a finite operating temperature range, it is necessary to ensure that the satellite's operating temperature falls within this range, otherwise components could be damaged, leading, in the worst case, to mission failure.

4.2.2.1 Temperature Range

The different temperature ranges for the different components are shown in Figure 12.
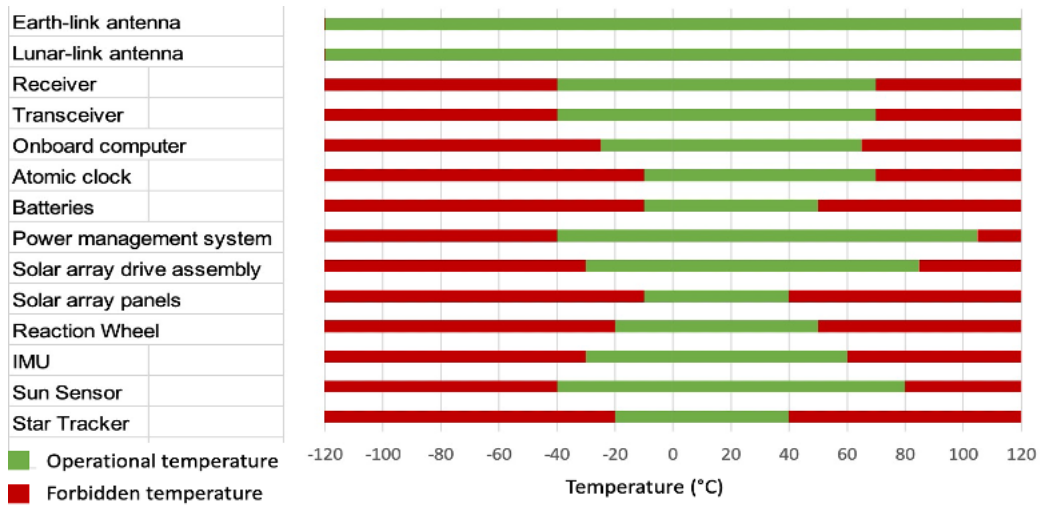
Figure 12: Temperature range of each component

If we analyze Figure 12, we first realize that the limiting component is the solar panel. However, it is worthwhile to qualify this interval. The solar panel can withstand large temperature differences, but this is at the expense of its efficiency. This being said, we try to place ourselves at the maximum efficiency of the solar panels in order to take full advantage of them, namely a temperature of 28°C.

4.2.2.2 Single Node Model

For thermal analysis, the simple node model is used, which consists of analyzing all the heat flows into the spacecraft, Q_{in}, as well as the heat flows out, Q_{out}, and assuming that these two flows are equal. The inflow is the sum of the heat flux from the spacecraft environment, Q_{env}, and the heat generation from the operation of components inside the satellite, Q_{sys}.

The environmental heat flow is given as described in equation 5.

$$Q_{env} = \alpha S(A_s + RA_p) + \alpha I A_p \quad (5)$$

Where α is the surface absorptivity, S is the solar flux, A_s is the sun facing projected area, R is the albedo (the percentage of solar flux reflected by

the Moon), A_p is the Moon-facing projected area, and I is the infrared radiation flux.

The subsystem heat generation follows the following equation:

$$Q_{sys} = \sum (1 - \mu_i) P_i$$
$$(6)$$

Where μ_i is the subsystem i's efficiency and P_i is its consumed power. Finally, the heat flows out, Q_{out}, can be obtained through equation 7.

$$(7)$$
$$Q_{out} = \sum (A_{ri} \epsilon_i) \sigma T^4$$

Where A_{ri} is the surface radiating area, ϵ_i is the surface emissivity, and σ is the Boltzmann constant. Thus, to know the temperature, we use the equality between inflows and outflows:

$$(8)$$

$$T = \sqrt[4]{\frac{Q_{env} + Q_{sys}}{\sum (A_{ri} \epsilon_i) \sigma}}$$

4.2.2.3 Thermal Scenarios

Having established and understood the equations, it is now a matter of determining the different thermal scenarios to which the spacecraft may be subjected. We identify two extremes, the hottest and the coldest cases. However, it must be borne in mind that these are extreme cases that will

not necessarily occur and that they correspond to the combination of extreme situations.

4.2.2.3.1 Hottest Case

The spacecraft is assumed to be at the closest point in its orbit to the Moon. It is oriented so that the -X Face sees the sun. The solar panels are rotated so that the entire surface faces the sun. Similarly, the opposite side of the solar panels and +X Face see the Moon. We place the satellite in the operational mode that consumes the most power in order to maximize $Q_{sys} = 35.72$W. It is assumed that all power consumed is eventually lost as heat (i.e., $\mu_i = 0$).
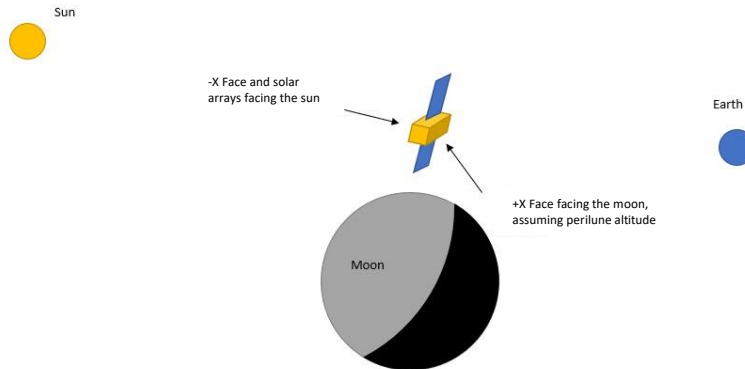

Figure 13: Hottest case scenario

4.2.2.3.2 Coldest Case

In this scenario, the satellite is in the Moon's shadow. It always presents the same face to the Moon as before. Moreover, the satellite is located at the furthest point of its orbit from the Moon (aplune). Finally, the satellite should be in the most economical operating mode (Safe Mode, 10.92 W).

Figure 14: Coldest case scenario

4.2.2.3.3 Physical Parameters

The physical parameters used for the calculations are given here in Table 7.

Table 7: Physical parameters from the Sun and the Moon for thermal analysis

Solar flux at the moon	1,416.6 W/m² [13]
Moon albedo R	0.07
Average Lunar IR Flux	430 W/m²
Perilune	2,616.56 km
Aplune	10,466.24 km

4.2.2.4 Operating Temperature and Materials Used

The different materials used to thermally protect the spacecraft and its components are presented. The difficulty encountered was that it was necessary to both dissipate heat to the outside during the hot phase and try to capture a maximum of heat during the cold phase without re-emitting too much afterwards.

Table 8: Coating parameter chosen for each external surface

Component	Materials used	Absorptivity α	emissivity ϵ
+X and - X Faces	Anodized Aluminum	0.25	0.25
+Z and - Z Faces	Anodized Aluminum	0.25	0.25
+Y and - Y Faces	Anodized Aluminum	0.25	0.8
Solar arrays	Solar cell	$0.88 \times (1 - \mu_{solar\ cell})$ $= 0.88 \times (1 - 0.307)$	0.84
Solar panel (without arrays)	S13G-LO	0.2	0.85
Antenna	Bare aluminum	0.09	0.1
Star tracker	8mm quartz mirror	0.05	0.8
Sun sensor	8mm quartz mirror	0.05	0.8
Xenon tanks	Multilayer insulation	0.34	0.55

We have assumed here that 88% of the incident radiation is absorbed by the solar cells. 30.7% of this radiation is then converted into electricity. The remaining energy is then used in the thermal balance of the spacecraft.

This gives a maximum temperature of 37.2°C which is below the lowest maximum temperature allowed by the components. It corresponds to an extreme case, which is therefore satisfactory. With such material parameters, the coldest temperature would then be -129°C. The solution for increasing the temperature is to use heaters. The chosen model is the All-Polyimide Thermofoil™ Heaters: HAP6944, whose characteristics are described in Table 9.

Table 9: Heater specifications

Diameter	12.7 mm
Thickness	0.76 mm
Weight	4.5 g
Resistance	37.9 Ω
Voltage	4 V
Power	12 W

If 10 heaters are used, then a power dissipation of 120 W is expected, which allows the spacecraft to be warmed up to a temperature of -9°C. Again, this is the worst possible case. It was also confirmed that the battery could deliver enough energy to ensure that the heaters would work without interruption, even during the longest eclipses (in the shadow of the Earth, for example).

4.2.3. Attitude Determination and Control subsystem (ADCS)

The attitude determination and control system has three main functions: to compensate for angular velocities introduced by the launch vehicle at the separation stage, to compensate for disturbances torques, and to perform angular maneuvers to adjust the satellite orientation for the different operation modes (propulsion maneuvers, sun acquisition, telemetry, etc.). Since non-steerable antennas are used, their directional gain relies on the spacecraft's attitude.

4.2.3.1 Sensors

In order to successfully determine and control the spacecraft's attitude, star trackers, sun sensors, and an IMU are installed on each spacecraft. The IMU is used to provide measurements which enable it to act as a navigation instrument. The spacecraft's attitude is estimated by means of an extended Kalman filter (EKF), using orientation information provided by the star tracker, sun sensors, gyroscope, and accelerometer. The gyroscope and accelerometer are integrated parts of the IMU.

Based on the radiation pattern of the transmitting antennas on each spacecraft, the estimated requirement for attitude precision is on the order of 2.5°. Considering the necessary attitude precision for the maneuvers, navigation and specific positions, the system can achieve a precision of around 0.1°. Information on the sensors is presented in Tables 10 - 12.

Table 10: Star Tracker Specifications

Model	ST400
Accuracy (pitch, yaw)	10 arcsec (3σ)
Accuracy (roll)	120 arcsec (3σ)
Sun exclusion half angle	40 deg
Unit	1

Table 11: Sun Sensor Specifications

Model	Red Wire Digital Sun Sensor
Field of View	±32 × ±32 deg
Accuracy	0.1 deg
Unit	2

Table 12: IMU Specifications

IMU	MEMS Gyro	Accelerometer	Inclinometer
Input Range	±400 deg/sec	±10 g	±1.7 g
Resolution	0.22 deg/h	1.9 μg	0.2 μg
Bias Instability	0.3 deg/h	0.05 mg	x
Random Walk	0.15 deg/$\sqrt{h}$	0.07 m/s$\sqrt{h}$	x

4.2.3.2 Disturbance Torque

There are three main sources of disturbance torque to the MORSE spacecraft: Lunar gravity gradient, solar radiation pressure, and the spacecraft's own main thruster during ΔV burns.

Lunar gravity gradient is caused by small differences in the Moon's gravitational force on each point of the spacecraft on different portions

of the orbit, which leads to a torque T_g. The formula for obtaining T_g is given by Equation 9.

$$T_g = \frac{3\mu}{R^3} \boldsymbol{u} \times (\boldsymbol{I} \cdot \boldsymbol{u}) \qquad (9)$$

Where μ is the standard gravitational parameter for the Moon ($\mu = 4.904 \times 10^{12}\ m^3 s^{-2}$), R is the orbit radius, $\boldsymbol{u}$ is the unit vector from the center of the Moon to the center of gravity of the spacecraft, and $\boldsymbol{I}$ is the spacecraft's moments of inertia to each axis of rotation.

Meanwhile, solar radiation pressure disturbance is due to the momentum transfer between photons emitted by the sun and their respective impact points on the spacecraft, which may lead to a torque T_s. The torque disturbance T_s is given by Equation 10.

$$T_s = P_s(1+q)cos(\phi)\ \boldsymbol{r} \times \boldsymbol{S} \qquad (10)$$

Where P_s is the effective solar radiation pressure ($P_s = 4.5567 \times 10^{-6}\ N \cdot m^{-2}$), q is the reflectance constant ($q = 0.6$), ϕ is the maximum angle of incidence of the sun ($\phi = 0°$), $\boldsymbol{r}$ is the vector from the geometric center to the center of mass, and $\boldsymbol{S}$ is the considered surface area multiplied by its corresponding unit normal vector.

Finally, the main thruster induced torque occurs due to a non-alignment between the thrust vector and the center of mass of the spacecraft. The moment arm will induce a torque to the spacecraft whenever the main thruster is operating, i.e., during ΔV burns. An important aspect to consider is that the center of mass of the spacecraft is not static through the burning time due to the mass flow of the propellant.

By analyzing the center of mass position in different time steps of the ΔV burn, the motion of the center of mass can be approximated by a linear function as shown in Figure 15. Therefore, a linear approximation of the disturbance torque over time can be obtained during propulsion mode and is depicted in Figure 16.

4.2.3.3 Actuators

Two types of actuators were selected to compensate for disturbances and perform angular maneuvers: reaction wheels and reaction control thrusters.
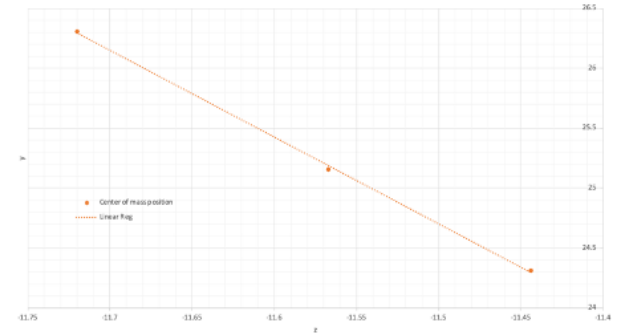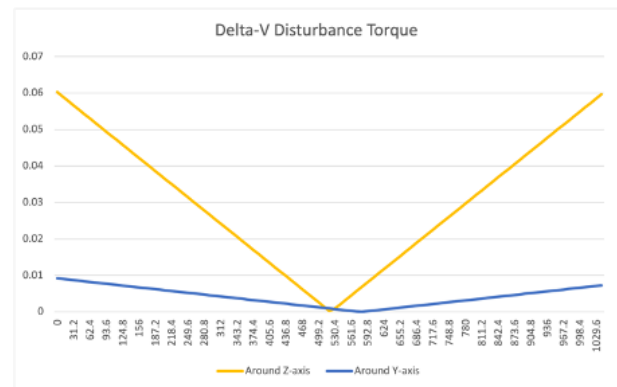

Figure 15: Center of mass motion over ΔV burn.

Figure 16: Main thruster disturbance torque (Nm) in 2-axis during propulsion mode operation (1040s).

4.2.3.3.1 Reaction Wheels

For general maneuvers and suppression of gravity gradient or solar radiation pressure disturbance torques, four reaction wheels are employed as actuators. This decision was based on their generated torque, momentum, and endurance through the mission life. Those characteristics are listed in Table 13.

Table 13: Specifications of Reaction Wheels

Model	Blue Canyon Technologies RPW050
Momentum	0.05 Nms

Max Torque	0.007Nm
Design Life	>5 years

4.2.3.3.2 Reaction Control System

The reaction control system (RCS) is composed by four reaction control thrusters (RCTs) located on the -X face of the spacecraft. From Figure 15 it is possible to see two clear intervals for each axis (4 in total) in which disturbance torque is present. Each of these intervals correspond to the active region of one of the four reaction thrusters. Since its sole purpose is to compensate for the ΔV disturbance, RCS is only active when the main thruster is active, and the activated RCTs at a given time are determined by the current time in the ΔV burn. For example, at $t = 300s$, RCT 1 and RCT 3 are active. The active intervals for each RCT and general specifications are given in Table 14.

Table 14: Specifications of Reaction Control Thrusters

	RCT 1	RCT 2	RCT 3	RCT 4
Δt_0 (s)	0	522	0	580
Δt_f (s)	522	1040	580	1040
T_{Avg} (N)	0.22	0.14	0.04	0.03
m_p(g)	425	268	86.4	58.5
Propellant		Xenon		

4.2.3.4 Momentum Unloading

A general concern with reaction wheels is related to the saturation of the wheels during the mission time, which could lead to disastrous responses and even mission failure. For the wheels to saturate, the amount of torque introduced to the spacecraft has to be enough for the wheels to reach their maximum rotational speed. To assess that, a careful study was conducted regarding the influence of the relevant disturbance torques on the spacecraft over one orbit of the Moon around the Earth. Considering the worst-case scenario in which T_g is constantly at its maximum value on each rotation axis (not realistic, but acceptable for designing purposes), the total disturbance torques the reaction wheels must compensate for was found to be:

$$T_{Max} = \begin{bmatrix} 9.78 \times 10^{-8} \\ 1.09 \times 10^{-7} \\ 4.82 \times 10^{-7} \end{bmatrix} \text{Nm}$$

The percentage of the storage momentum for the z-axis reaction wheel along one cycle is depicted in Figure 17. As it can be seen, the torque around the z-axis is more severe than the others and, even so, less than 2.5% of the total momentum storage capability is achieved over that time. With a maximum momentum storage percentage of only 2.41% for the worst-case scenario due to the disturbance torques and considering the physical limitations required by the spacecraft for this mission, a strategy to unload the reaction wheels in 3-axis was not included.
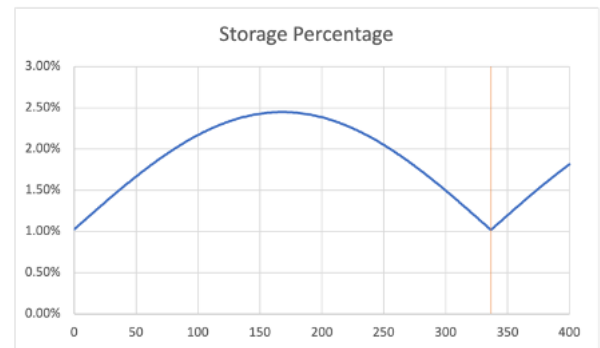

Figure 17: Percentage of maximum momentum storage in use by z-axis reaction wheel over a cycle (until red line).

4.2.3.5 Attitude Control

The control strategy adopted is based on the zero-momentum control method and makes use of a quaternion representation for the attitude

parameters [14]. Consider a unit vector $\hat{e} = [e_1 \; e_2 \; e_3]^T$ as the Euler axis and an angle of rotation φ (Euler angle) on the inertial frame. The associated quaternion components are defined as:

$$q = \begin{bmatrix} q_1 \\ q_2 \\ q_3 \\ q_4 \end{bmatrix} = \begin{bmatrix} e_1 \sin\left(\frac{\varphi}{2}\right) \\ e_2 \sin\left(\frac{\varphi}{2}\right) \\ e_3 \sin\left(\frac{\varphi}{2}\right) \\ \cos\left(\frac{\varphi}{2}\right) \end{bmatrix} \quad (12)$$

The quaternion column vector q then represents an attitude maneuver of the spacecraft on the inertial frame. It is then possible to observe that the quaternion comprises one scalar part $S(q) = q_4$ and a vector part $V(q) = [q_1 \; q_2 \; q_3]^T$. By defining the angular velocity of the spacecraft on the inertial frame $\omega = [w_x \; w_y \; w_z]^T$, the derivative of the quaternion becomes:

$$\dot{q} = \frac{1}{2}\omega^{\times}q \quad (13)$$

Where $\omega^{\times}$ represents the 4x4 skew symmetric matrix of ω.

The dynamics of the spacecraft is defined by the laws of rotational mechanics, which is expressed through Equation 14.

$$I\frac{d\omega}{dt} = \omega \cdot (I\omega + h_w) - \frac{dh_w}{dt} + T_d \quad (14)$$

Where I is the inertia matrix of the spacecraft, h_w is the angular momentum of the reaction wheels, and T_d is the disturbance torque.

Finally, for feedback control input, two gains, K_1 and K_2, were considered and optimized in the simulation environment. The gain K_1 is

associated with the vectorial part of the quaternion error $(q_e) = V(q_c^{\times}q)$, where $q_c^{\times}$ represents the skew symmetric matrix of the command (desired) quaternion. K_2 is related to the angular velocity ω. The control input u is given by Equation 15:

$$u = -K_1 \cdot V(q_c^{\times}q) - K_2 \cdot \omega \quad (15)$$

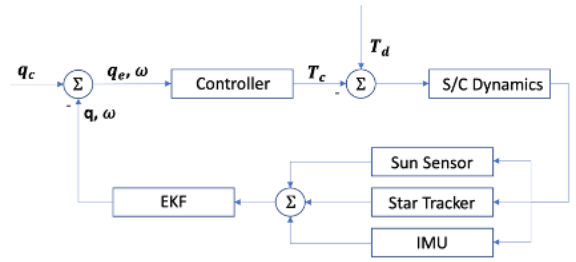Where $K_1 = 0.05$ and $K_2 = 0.215$. The schematic for the ADCS is represented in Figure 18.

Figure 18: MORSE's ADCS schematic without RCS, T_c and T_d represent the control and disturbance torques respectively.

4.2.3.6 Simulation

A simulation was conducted on the MATLAB/SIMULINK environment to assess the performance of the control system and verify that the appropriate choice of actuators was made. Three scenarios were considered in the simulation: detumbling, position maintaining and angular maneuver. The launch vehicle's reaction control gas system can introduce a one-axis spin of 5 rpm in a clockwise or counterclockwise direction before spacecraft separation. The results for this scenario are expressed in Figures 19 and 20. Angular velocity and quaternion error values suggest that detumbling can be achieved in less than 60 seconds.
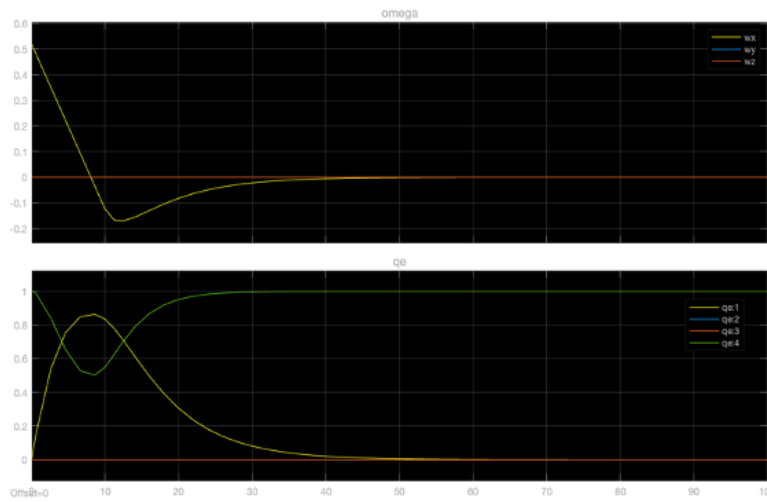
Figure 19: Angular rate (rad/s) and quaternion error over time (s) for detumbling.
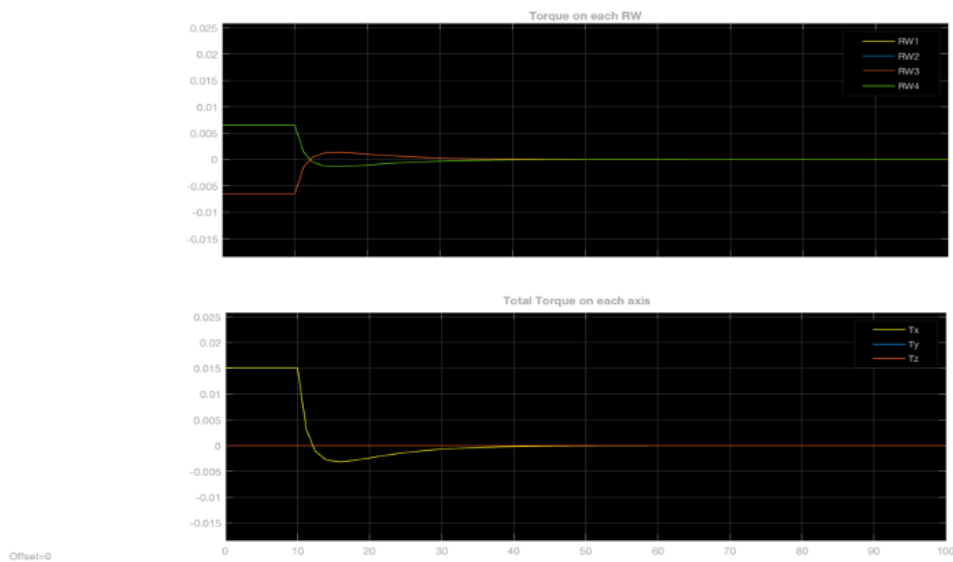

Figure 20: Reaction wheels' torque and total torque (Nm) for detumbling over time (s).

The second scenario simulated was positioning maintenance in the presence of disturbances. For that simulation, a perturbation with the maximum disturbance torque in all axes was considered and the angular velocity and Euler angles are presented in Figure 21. The maintenance of the current attitude is very well achieved in the presence of disturbances.

The final scenario simulated is an angular maneuver. The maneuver selected corresponds to a 90º rotation through the z axis. Such maneuver can be required for a change in operation modes or a sweep to obtain sun sensor information, for example. The results of the simulation are shown in Figure 22. The simulations indicate good results for our choice of components.
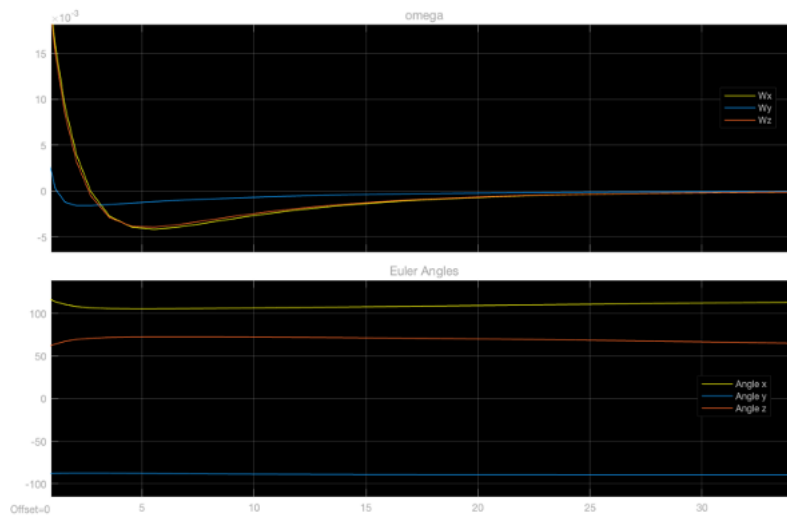
Figure 21 Angular velocity (rad/s) and Euler angles (degrees) over time (s) for attitude maintenance in the presence of disturbances.
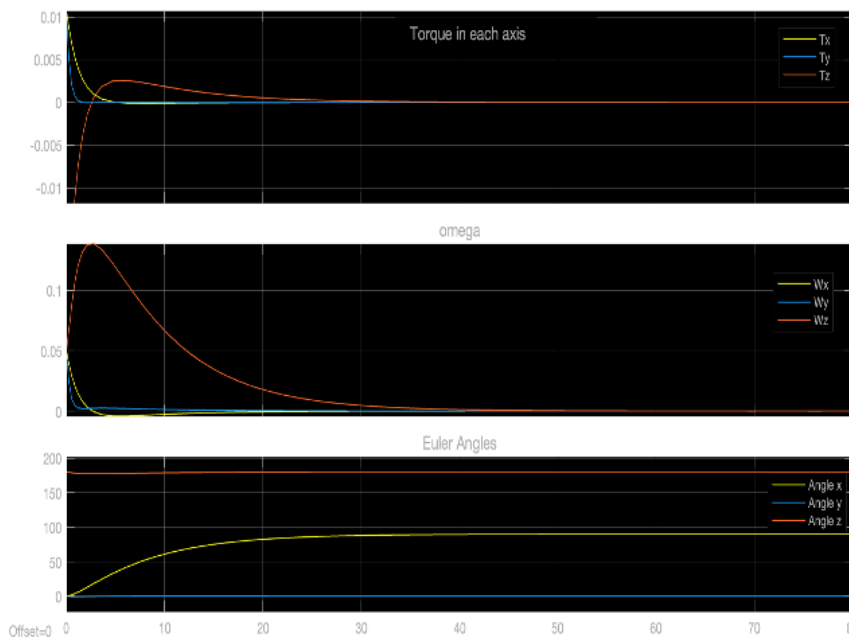
Figure 22: Torque in each axis (Nm), angular velocity (rad/s) and Euler angles (degree) over time (s) for attitude maneuver of 90º.

4.2.4. Electrical Power Subsystem (EPS)

The electrical power system consists of solar array panels, a power distribution system, and batteries. It generates, stores, and distributes electrical power to all subsystems of the spacecraft. A block diagram of the electrical power system is shown in Figure 23.
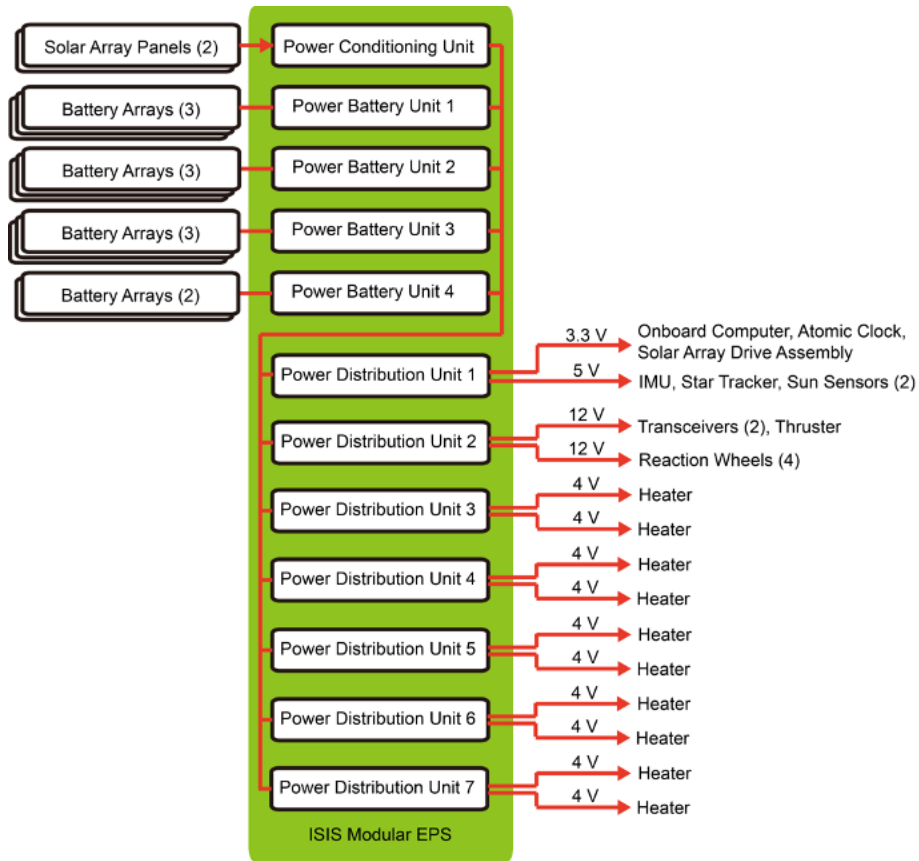
Figure 23: Block diagram of the electrical power system

4.2.4.1 Operational Modes and Power Demand

The status of each subsystem and the maximum power demand of each operational mode are summarized in Table 14. Section 4.4 gives a detailed explanation of the operational modes.

In the mission orbit, whose period is 47,464 s, each spacecraft has line of sight with the Lunar South Pole for about 36716 s, or 77.4% of the time, according to our simulation in STK. For power-related estimations, we assume that each spacecraft's time in line-of-sight is evenly split between Positioning Mode and Relay and Positioning Mode, 10% of its time outside of line-of-sight is spent in Telemetry and Tracking Mode, and the rest is spent in Safe Mode (Figure 24). Under these assumptions, the electrical energy demand in one orbit can be calculated as follows:

36,716 s x 0.5 x (35.72 W + 23.92 W) + (47464 s - 36716 s) x (0.1 * 22.72 W + 0.9 x 10.92 W) = 1,225,000 J = 340.3 Wh.
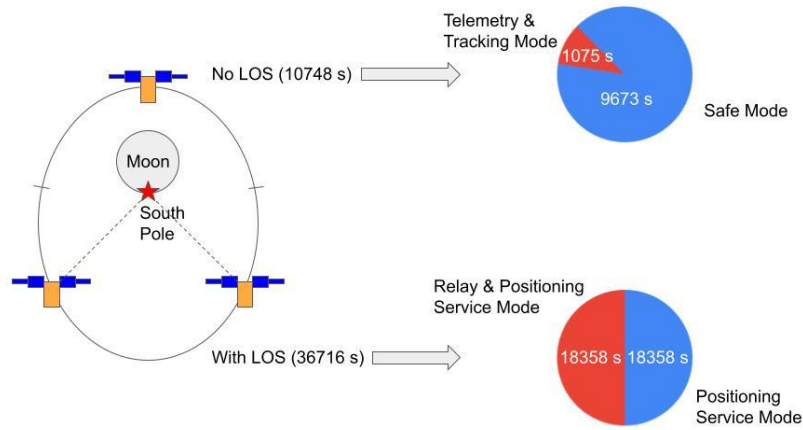
Figure 24: Assumed durations of operational modes over one orbit

Table 14: Subsystem status and maximum power demand of each operational mode

Subsystem	Component	Maximum Power Demand (W)	Operational Mode						
			Launch	Detumbling	Propulsion	Relay & Positioning Service	Positioning Service	Telemetry & Tracking	Safe
TT&C	Transmitter (Earth)	11.8	OFF	ON	ON	ON	OFF	ON	OFF
	Receiver (Earth)	1.2	OFF	ON	ON	ON	ON	ON	ON
	Transmitter (Moon)	11.8	OFF	OFF	OFF	ON	ON	OFF	OFF
	Receiver (Moon)	1.2	OFF	OFF	OFF	ON	ON	OFF	OFF
	Atomic Clock	0.12	ON	ON	ON	ON	ON	ON	ON
ADCS	Sensors	5.2	OFF	ON	ON	ON	ON	ON	ON
	Reaction Wheels	3	OFF	ON	ON	ON	ON	ON	ON
C&DH	Onboard Computer	0.4	ON	ON	ON	ON	ON	ON	ON
Propulsion	Thruster	70**	OFF	OFF	ON	OFF	OFF	OFF	OFF
EPS	SADA	1	OFF	OFF	ON	ON	ON	ON	ON
Maximum Power Demand (W)			0*	21.72	92.72**	35.72	23.92	22.72	10.92

*Power provided by launch vehicle.

**Only when valves are opening/closing; maximum sustained power demand of the Propulsion Mode is 22.72 W.

4.2.4.2 Power for Thermal Control

According to our thermal calculations shown in Section 4.2.2, when a spacecraft is in umbra, 130.92 W of heat will be needed to keep the temperature within operational limits, but onboard components cannot not generate enough waste heat for the purpose. Heaters will be required to make up for the difference. 10 heaters will consume up to 120 W of power and generate the same amount of heat.

4.2.4.3 Solar Lighting Condition

The spacecraft will encounter shadows cast by the Moon or the Earth. The Moon's shadow will be more frequently encountered but given the mission orbit's high eccentricity and inclination, the time spent in the Moon's shadow will be relatively short (less than 1h 4m), so we design the spacecraft to be able to continue normal operation during eclipses by the Moon and recharge the batteries within the same orbit. On the other hand, the Earth's shadow can produce much longer eclipse times but the frequency of encountering it is much lower. The Moon encounters the Earth's shadow during Lunar eclipses. Table 15 summarizes all Lunar eclipse events in the five-year planned mission duration from November 2023 to November 2028. The longest Lunar eclipse in the timeframe will occur on March 14, 2025, during which the Moon will be in the Earth's shadow for 6h 2m 37s, of which 3h 38m 15s is in the umbra and the rest in the penumbra. We assume that the same shadowed time will occur to the spacecraft. Since Lunar eclipses are relatively rare, while more battery capacity will be provided for the events, a brief service disruption afterwards for recharging the batteries will be accepted.

Table 15: Lunar eclipses during the planned mission duration (Nov 2023-Nov 2028)

Date	Eclipse Type	Penumbra Duration	Umbra Duration
2024 Mar 25	Penumbral	4 h 39 m 07 s	N/A
2024 Sep 18	Partial	4 h 06 m 16 s	1 h 02 m 47 s
2025 Mar 14	**Total**	**6 h 02 m 37 s**	**3 h 38 m 15 s**
2025 Sep 07	Total	5 h 26 m 40 s	3 h 29 m 24 s
2026 Mar 03	Total	5 h 38 m 37 s	3 h 27 m 10 s
2026 Aug 28	Partial	5 h 37 m 46 s	3 h 18 m 07 s
2027 Feb 20	Penumbral	4 h 00 m 59 s	N/A
2027 Jul 18	Penumbral	0 h 11 m 47 s	N/A
2027 Aug 17	Penumbral	3 h 38 m 35 s	N/A
2028 Jan 12	Partial	4 h 10 m 41 s	0 h 56 m 00 s
2028 Jul 06	Partial	5 h 10 m 38 s	2 h 21 m 30 s

(Source: [15])

4.2.4.4 Solar Array Panels

Sun-tracking solar panels will be used for the mission so that the spacecraft can rotate in the desired direction for communication while maintaining maximum solar power generation. To ensure normal operation during an eclipse by the Moon and replenishment of the batteries within one orbit, an orbit containing the longest Moon eclipse time (1h 4m) is considered for estimating the required solar power generation capacity. We assume that the eclipse happens when the spacecraft is in Safe Mode, which is both the worst case since the heater will need to supply the most power and the most likely case since an eclipse is more likely to happen when the spacecraft is close to the Moon near the perilune. When the eclipse happens, the heater needs to provide 130.92 - 10.92 = 120 W of heat for 1h 4m, making the total energy demand 1,687,000 J. The time for solar power generation in that orbit is reduced by 1h 4m to 11h 59m 28s. Assuming a 90% efficiency of the power distribution system, the minimum end-of-life (EOL) power generated by the solar array panels (P_{EOL}) can be calculated as:

$$\frac{Energy}{Time} = Power \Rightarrow \frac{1687000\ J}{43168\ s} = 39.08\ W \quad (16)$$

The required beginning-of-life (BOL) power generation capacity (P_{BOL}) can then be calculated by the following equation:

$$P_{BOL} = P_{EOL}\ (1 - D)^{-Y} \quad (17)$$

Where D is the degradation rate per year and Y is the number of years since BOL. Assuming a degradation rate of 3.75% per year and a mission duration of 5 years, the required P_{BOL} is 47.31 W. The MMA Design HaWK 17AS56 solar array

panels (specifications summarized in Table 16) can generate 56 W of power in BOL, more than enough to satisfy the requirement.

The solar array consists of a pair of deployable wings attached to a solar array drive assembly that allows sun-tracking movement around one axis. The sun-tracking solar array panels mounted in the ±Z direction allows the spacecraft to rotate around its Z axis while the solar array panels are facing the sun. By also rotating the spacecraft in the plane of the solar array panels, the spacecraft can point an antenna in any desired direction. Each wing of the solar array contains 28 solar cells. Various configurations of the HaWK solar array panels have flight heritage on missions including the deep-space CubeSat MarCO, and the same 17AS56 sun-tracking version will fly on several secondary payloads of the Artemis 1 mission including the Japanese EQUULEUS spacecraft.

Table 16: Specifications of the HaWK 17AS56 solar array panels

Mass	361g*
Size (Stowed, each wing)	337 x 89 x 9 mm
Size (Deployed, each wing)	624 x 226 x 2 mm
Solar Cell	Spectrolab XTJ Prime
Solar Cell Efficiency	30.7%
Number of Solar Cells	56*
Power Output (BOL, 1 AU)	56 W*
Power Output (EOL, 1 AU) **	46.26 W

*2 wings combined

**After 5 years with 3.75% degrade rate per year

4.2.4.5 Power Distribution System and Batteries

The ISIS Modular EPS, a COTS power distribution system and battery package with flight heritage, is selected for the mission. The system consists of one or more modular Power Conditioning Units (IPCU), Power Battery Units (IPBU), Power Battery Packs (IPBP), and Power Distribution Units (IPDU). The IPCU can accept inputs from up to four solar panel channels each generating 39 W, satisfying the mission's need for two solar panels producing a total of 56 W. Seven IPDUs will be installed on each spacecraft. Two of the IPDUs will output power in 3.3V, 5V, and 12V channels to all onboard components except for the heaters. The remaining five will each supply two 4V channels to the heaters. The high current requirement (3A) limits the number of heaters that can be connected to one IPDU to a maximum of two.

An IPBU can be interfaced with up to three batteries. Instead of the standard IPBPs, we selected the EXA 50 Whr High Energy Density Battery Array for its more compact volume and lower mass for a similar capacity. Each battery array has a capacity of 44.4 Wh, a maximum charge rate of 20.5 W, and a maximum discharge rate of 68.3 W. Three arrays can accommodate the maximum surplus power from the solar arrays (45.08 W during Safe Mode in BOL) and discharge enough power to supply the maximum power demand of 130.92 W. To estimate the battery capacity needed to constantly supply enough power to the spacecraft, we conducted a simulation of the drained battery capacity in the most demanding situation: the March 14, 2025,

Lunar eclipse. In the simulation, solar intensity during penumbra was assumed to be 50% of the normal intensity under full sunlight, so solar power output during penumbra was also halved. In order to test the worst-case scenario, EOL solar panel performance was used. To account for power loss from the power distribution system, a further 10% was subtracted from the EOL solar panel output. The drained battery capacity at the end of each time step was calculated using Equation (18):

$$C_i = C_{i-1} + t(P_{generated} - P_{consumed}) \ (18)$$

Here C_i and C_{i-1} are the drained capacities after and before the time step, respectively, with C_{i-1} starting from 0 initially, representing a full battery; $P_{generated}$ and $P_{consumed}$ are the generated and consumed power during the time step, respectively; and t is the length of the time step.

The result from the simulation in Figure 24 shows that 475.68 Wh of energy will be drained from the batteries over the course of the eclipse. By entering Safe Mode during penumbra and until normal operation can resume, the charging rate is maximized. The drained battery capacity can be replenished in around 21 hours after the start of the eclipse and normal service can be resumed. Based on NASAs Lunar eclipse data, we expect five events of service suspension over the entire 5-year mission duration, each lasting less than a day. To provide more than 475.68Wh of battery capacity each spacecraft will be equipped with 11 battery arrays totaling 488.4 Wh capacity each. 4 IPBUs will interface them with the power distribution system.
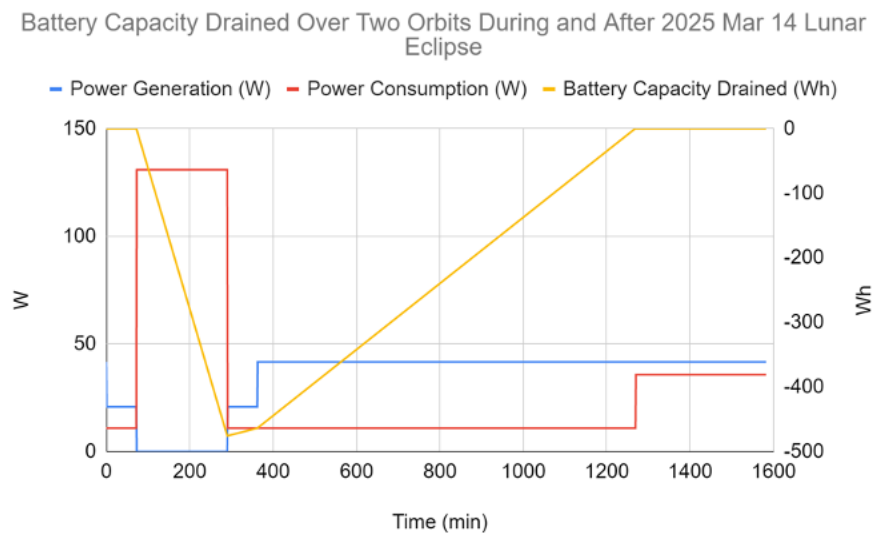
Figure 25: Simulation result for drained battery capacity over two orbits during and after the longest Lunar eclipse. [11]

4.2.5. Command and Data Handling Subsystem (C&DH)

The command and data handling system will perform the following operations:

- Command the power distribution system to initiate subsystems required for the Detumbling Mode after receiving indication of successful separation from the launch vehicle.
- Receive and execute commands from Earth ground stations to switch among operational modes
- Monitor the status of each subsystem and command the spacecraft to enter Safe Mode if any anomaly is detected.
- Collect telemetry from each subsystem, format the data, and command the transceiver to downlink it to ground stations.
- Receive and process data from attitude sensors and control reaction wheels to achieve the desired attitude.
- Process attitude data from sensors and positional information from ground stations, determine the best antenna for Lunar or Earth link, and connect it to the transceiver.
- Retrieve time signal from the atomic clock and command the transceiver(s) to broadcast it for positioning service and tracking by ground stations.
- Receive time signal from the ground stations and calibrate the atomic clock.
- Receive and carry out any additional commands from ground stations

The ISIS Onboard Computer will provide C&DH functions to the spacecraft. The computer will interface with all subsystems by I^2C buses for data transfer in both directions. Specifications for the ISIS Onboard Computer are summarized in Table 17.

Table 17: Specifications of the ISIS Onboard Computer

Size	96 x 90 x 12.4 mm
Mass	100 g
Processor Clock Speed	400 MHz
Volatile Memory	64 MB
Code Storage	1 MB
Critical Data Storage	256 kB
Mass Data Storage	2 x 2 GB (redundant)

4.2.6. Telemetry, Tracking and Command Subsystem (TT&C)

The TT&C subsystem serves multiple purposes for the MORSE mission. The foremost reason is to provide the mission objective - the relay and positioning service. This subsystem also provides full duplex communications with Earth ground stations for spacecraft commands and telemetry.

The positioning service provided uses a two-satellite positioning method based on Multi-Epoch Double-Differenced Pseudorange Observations (MDPO) [10]. The specified orbit will ensure that 2 satellites will be in view of the South Pole at all times, allowing this method to be employed.

To fulfill the requirement of simultaneously communicating with rovers and ground stations, two transceivers are used to handle uplinks from both sides.
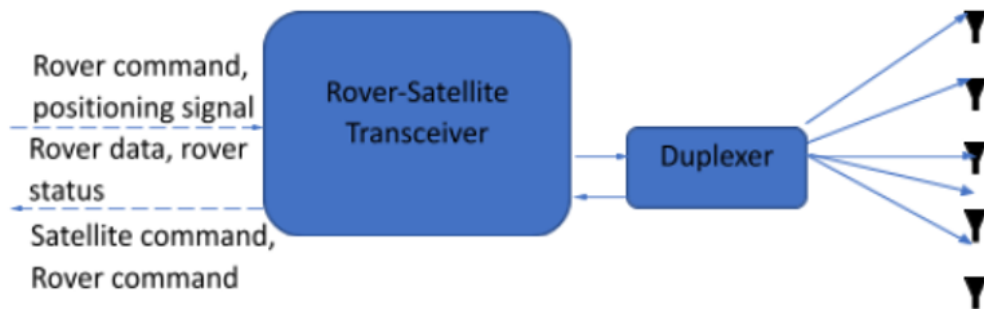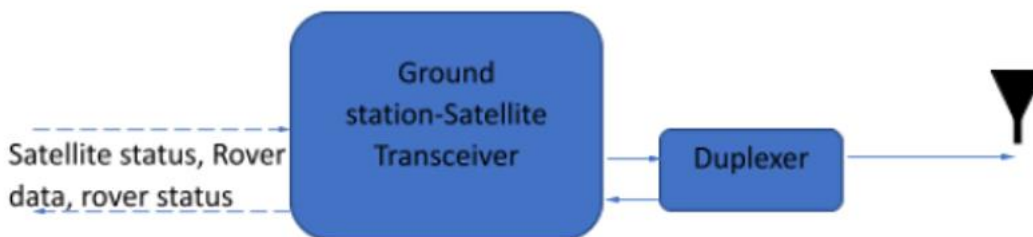

Figure 26: Rover-to-satellite

Figure 27: Ground station-to-satellite

The TT&C system provides its services depending on the operational mode that it is in. These modes align with the operational modes in Section 4.4.
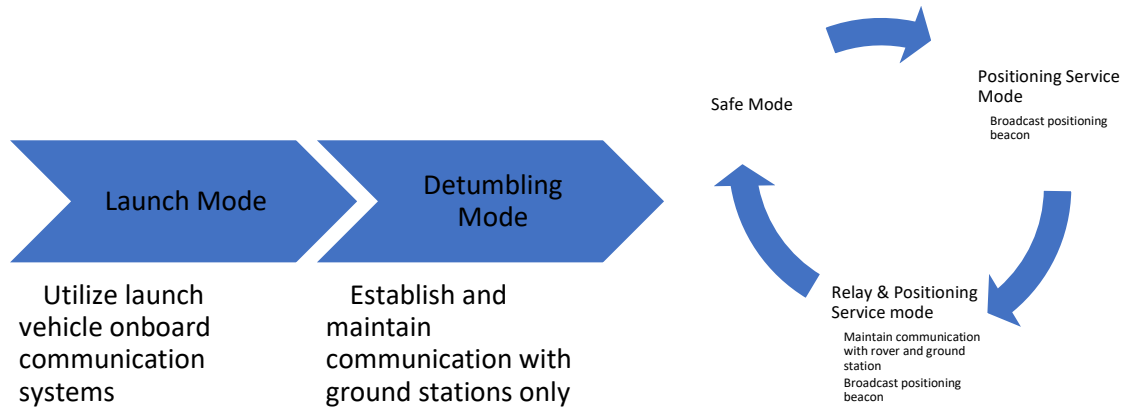
Figure 28: Operational modes

4.2.6.1 Link Budgets

4.2.6.1.1 Earth-Satellite

As the distance from the spacecraft to Earth ground stations is very large, there is a great loss in signal strength; however, the very large high-gain antennas of the NEN allow for the reception of very faint signals. The system has an uplink and downlink margin of 1.1 dB and 4.7 dB, respectively. This shows that signals can be successfully transmitted and received in both directions between the spacecraft and the ground stations. The small link margin indicates that unstable power supply or extra atmospheric attenuation, for example: rain, could cause the signal to become too noisy to read. While a higher gain antenna can be designed for this purpose, the use of COTS components limits the selection range.

Table 18: Link budget for Earth to satellite

Item		Uplink	Downlink
1	Transmitter Power (W)	N/A	3.000
2	Transmitter Power (dBW)	N/A	4.771
3	Frequency (GHz)	2.000	2.000
4	Transmitter Antenna Gain (dB)	N/A	6.500
5	Transmitter Feeder Loss (dB)	N/A	-2.000
6	Transmitter EIRP (dB)	65.000	9.271
7	Transmit distance (km)	384,400.000	384,400.000
8	Free Space Loss (dB)	-210.156	-210.156
9	Atmospheric Loss (dB)	-1.000	-1.000

10	Carrier Power Density (dBW)	-146.156	-201.885
11	Equivalent Noise Temperature (K)	135.000	135.000
12	Receiver Antenna Diameter (m)	N/A	9.100
13	Receiver Efficiency (%)	N/A	100%
14	Receiver Antenna Gain (dB)	6.500	65.817
15	Receiver G/Te (dBK-1)	-14.803	44.513
16	Receiver Feeder Loss (dB)	-2.000	-2.000
17	C/N0 (dB)	65.642	69.229
18	RF Bandwidth (MHz)	2.000	2.000
19	Spectral Efficiency (bits/s/Hz)	1.000	1.000
20	Filter Roll-off Factor	0.950	0.950
21	Maximum bit-rate (Mbit/s)	1.026	1.026
22	Eb/N0 (dB)	5.532	9.119
23	C/N (or SNR)	2.631	6.219
24	Link Margin	1.131	4.719

4.2.6.1.2 Moon-Satellite

To standardize the communication transmission power from the Lunar surface to the satellites, a client-side requirement is established. For customers to use MORSE's communication relay service, the uplink EIRP on the Lunar surface is specified to be 50 dB, and the receiving antenna should have a gain of 30 dB. This provides an uplink and downlink margin of 14.8 dB and 0.5 dB, respectively.

Table 19: Link budget for moon to satellites

Item		Uplink	Downlink
1	Transmitter Power (W)	N/A	3.000
2	Transmitter Power (dBW)	N/A	4.771
3	Frequency (GHz)	2.000	2.000

4	Transmitter Antenna Gain (dB)	N/A	6.500
5	Transmitter Feeder Loss (dB)	N/A	-2.000
6	Transmitter EIRP (dB)	50.000	9.271
7	Transmit distance (km)	8,000.000	8,000.000
8	Free Space Loss (dB)	-176.522	-176.522
9	Atmospheric Loss (dB)	0.000	0.000
10	Carrier Power Density (dBW)	-126.522	-167.251
11	Equivalent Noise Temperature (K)	135.000	135.000
12	Receiver Antenna Gain (dB)	6.500	30.000
13	Receiver G/Te (dBK-1)	-14.803	8.697
14	Receiver Feeder Loss (dB)	-2.000	-2.000
15	C/N0 (dB)	85.276	68.047
16	RF Bandwidth (MHz)	8.000	4.000
17	Spectral Efficiency (bits/s/Hz)	2.000	2.000
18	Filter Roll-off Factor	0.950	0.950
19	Maximum bit-rate (Mbit/s)	8.205	4.103
20	Eb/N0 (dB)	16.135	1.916
21	C/N (or SNR)	16.245	2.026
22	Link Margin	14.745	0.526

The components this system uses are 6 AnyWaves S-band patch antennas, 2 S-band transceivers, 2 amplifiers, a SP3T electronic switch, and the onboard computer for some processing. The specific patch antennas are chosen due to their operational frequency range, radiation pattern, and low weight and profile. The transceiver is compatible with the antennas and other common components that will be used on the rovers and landers, which will be using the provided service. The transceiver also employs the preferred modulation and error correction schemes which allow for low bit error rates (BER) and

signal reconstruction at the receiver in case of interference or major signal fading.

4.2.6.2 Wireless Communication

4.2.6.2.1 Multiple Access

A set of Gold code sequences will be used to provide direct-spreading code division multiple access (DS/CDMA). This will allow all users to operate on the channel simultaneously without interfering with each other's messages. Gold codes are a subset of pseudo-noise sequences that provide low cross-correlation and high auto-correlation, so no time synchronization is required. It is usually important for asynchronous CDMA systems to employ a method of power control to overcome the near-far problem. This problem, while being a major issue for mobile networks on Earth, will be of little significance to our proposed system, as the difference in distance between transmitters on the Lunar surface to our satellites will be relatively small compared to the total distance. Increasing the receiver dynamic range by using a higher resolution analogue-digital converter (ADC) can also provide extra support to solving this problem if necessary [16].

4.2.6.2.2 Modulation

Offset quadrature phase shift keying (OQPSK) modulation was chosen due to good spectral efficiency, compatibility with COTS components, and low error rate. The OQPSK modulation scheme encodes 2 bits of data into each symbol, allowing for twice the bitrate of BPSK provided the same baud rate. For the Earth-Satellite link, the interference from Earth-based sources, LEO satellite communication, and weather will contribute to random bit errors. This is why a low

error rate modulation such as OQPSK was chosen over a higher data rate modulation such as 16-QAM or higher. Due to the low level of noise between the satellite and the Lunar surface, less precautions are needed to be taken compared to traditional terrestrial communications. For simplicity, the same signal processing is done for all links. The bottleneck for data relaying will come from the data being sent to ground stations, so introducing a different modulation with a faster data rate for Lunar communications is redundant.

4.2.6.2.3 Error Correction

Due to random bit errors, some form of error correction is needed to recover a corrupted signal. A compromise is made between the resilience of error correction and the data rate. For each bit, some number of forward error correction bits are sent, with this number differing depending on the scheme used. For the purpose of our system, convolutional codes will be used. These codes are compatible with the transceivers being used and allow for a low signal-to-noise ratio (SNR) over the channel to be received successfully. Convolutional codes make use of Linear Feedback Shift Registers (LFSR). This hardware allows for the codes to be generated quickly and deterministically, while still appearing as pseudorandom noise. This system is built into the selected transceiver.

4.2.6.2.4 Communication protocols

For both the Lunar and Earth link, Disruption/Delay Tolerant Networking (DTN) will be used. DTN is ideal for this network as the connection is not necessarily continuous. This will ensure all data transmitted is received eventually. This is the protocol that is used by many satellites

that NASA has launched, and TCP systems in operational satellites are largely being upgraded to DTN [17]. This protocol relies on forwarding bundles of frames to the next closest available receiver. This allows 2 satellites within LoS of each other to pass bundles if one is not in LoS of a ground station. In the future, this protocol will support easier transmission to satellites at all altitudes of Earth orbit which will create an internet of space, whereby bundles can be forwarded many times to other satellites before arriving at the destination.
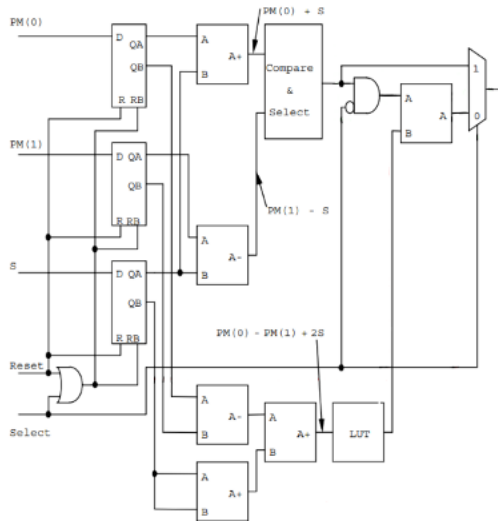

Figure 29: Hardware for convolutional codes

4.2.6.3 Communication and Attitude

In the Relay and Positioning Service Mode, in order to provide simultaneous communication relay in both Earth-satellite-Moon and Moon-satellite-Earth directions, the satellite should be able to point two different antennas at the Earth and the Moon. Due to the antennas' radiation pattern, the useful field-of-view for both Moon-satellite downlink and Earth-satellite uplink is limited to around $60°$ (gain ≥ 6 dB), which means that there is a $30°$ dead zone between each adjacent pair of antennas. As a result, in order to aim two separate antennas at the Earth and the Moon, the

two bodies need to be at least $30°$ apart as viewed from the satellite. We conducted a one-year simulation of two of our satellites in the General Mission Analysis Tool (GMAT). The result (that for the first month is shown in Figure 29) shows that there is at least one satellite in a position where the angular separation of the Earth and the Moon is larger than $30°$ at any given moment. Since the MORSE constellation is designed so that at least two satellites are constantly within LoS with the Lunar South Pole, it can provide uninterrupted relay service.
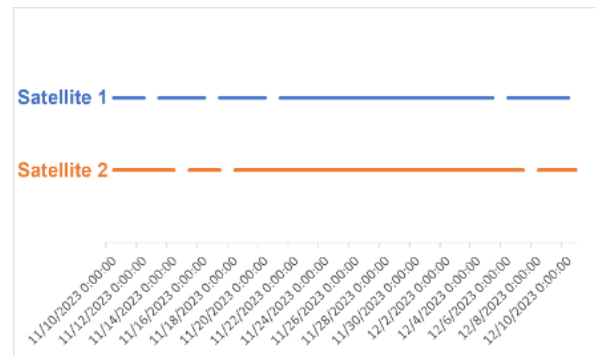

Figure 30: GMAT simulation result for the time when the angular separation of the Earth and the Moon is suitable for simultaneous communication (>30º), for two satellites located 120º apart in the mission orbit, over the first month of the planned mission time.

4.2.6.4 Positioning

To provide this proof-of-concept positioning service for rovers in the South Polar region of the Moon, the satellites with LoS will broadcast positioning signals when in range. The rovers or landers will receive and reply to these signals, and their distances can be determined using doppler ranging. With the satellite locations and distances to the rover known, it is possible to determine the rover's location to a relatively high accuracy and precision. The error is not expected to exceed 100m. This position information will be downlinked to both the rovers and ground stations

for processing and general path guidance, using the rover's onboard cameras and other sensors for smaller corrections. A rover or lander positioning beacon (depending on the lander design) can be used to increase the accuracy of this system. As a requirement, the rovers will process the positioning signal onboard.

The Earth's Global Positioning System (GPS) uses at least four signals to determine a location. The MORSE Positioning service provides two signals and hence a lower accuracy for the rover location. For future expansion of the capability, more MORSE satellites could be added to the orbit to provide a higher accuracy of the positioning service and higher redundancy of the overall system.

4.2.7. Propulsion Subsystem

The propulsion system includes a main thruster, its fuel tanks, and its pressurization equipment. The locations of the components in the spacecraft are shown in Figure 31. This system will provide the required ΔV for the Lunar orbit insertion (LOI) and orbital phasing maneuvers. Although the mission orbit is a frozen orbit that theoretically does not require any station-keeping, a ΔV margin is provided for station-keeping to account for perturbations not included in the theoretical calculations.
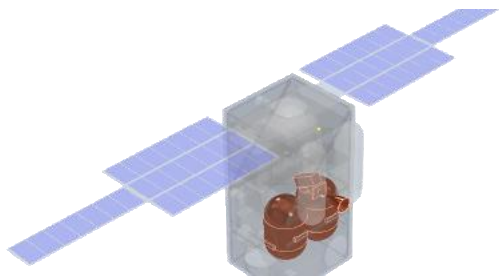

Figure 31: Locations of propulsion system components in the spacecraft

4.2.7.1 Main Thruster

The LOI maneuver sets the requirements for the main thruster. The relatively large ΔV requirement of 346 m/s and the limited mass budget for each spacecraft necessitate a high specific impulse. The time available for the LOI maneuver is limited because the spacecraft's velocity must be reduced to below the Lunar escape velocity before it leaves the Moon's Hill sphere on a hyperbolic flyby trajectory. A chemical bipropellant propulsion is chosen for the mission to provide high thrust and appropriately high specific impulse.

The selected main thruster is the ArianeGroup 10 N Bipropellant Thruster S10-13 (Figure 32), which has extensive flight heritage on both Earth-orbiting satellites and interplanetary probes since the 1970s [18]. Specifications of the thruster are summarized in Table 20. The main thruster will need to provide 440 m/s of total ΔV, including 346 m/s for LOI, 20 m/s for the phasing maneuver, with an added 20% for station-keeping and safety margin. Using a mix ratio of approximately 1.65, 0.91 kg of Monomethylhydrazine (MMH) and 1.49 kg of Dinitrogen Tetroxide (N_2O_4) will be required. Hydrazine-based bipropellant is chosen over green alternatives due to its higher energy density, specific impulse, and the availability of COTS thrusters with the appropriate mass and thrust. The risk associated with its toxicity is considered acceptable because the mission will be uncrewed and will not visit any potentially habitable environment.

Figure 32: The ArianeGroup 10 N Bipropellant Thruster S10-13. (Image credit: ArianeGroup)

Table 20: Specifications of the ArianeGroup 10 N Bipropellant Thruster S10-13

Mass	350 g
Nominal Thrust	10 N
Nominal Specific Impulse	292 s
Nominal Propellant Mix Ratio	1.60-1.65
Inlet Pressure Range	10-23 bar
Fuel	MMH
Oxidizer	N_2O_4

4.2.7.2 Tanks and Pressurization

Given the density of MMH is 0.875 g/cm^3 and that of N_2O_4 is 1.442 g/cm^3, the propellant tanks will need to hold 1,040 mL of MMH and 1030 mL of N_2O_4 to satisfy the mixing ratio. The tanks and pressurization system are custom-designed due to the lack of suitable COTS products. The propellant tanks are pressurized by xenon gas stored in two separate, highly pressurized tanks. Specifications of the tanks are summarized in Table 21.

Table 21: Specifications of Propellant and Pressurization Tanks

	Fuel Tank	Oxidizer Tank	Xenon Tank (per tank)
Size	D = 100 mm	D = 100 mm	D = 60 mm
	H = 65.75 mm	H = 64.48 mm	H = 151 mm
	t = 0.58 mm	t = 0.58 mm	t = 2.4 mm
Dry Mass	96 g	95.34 g	150 g
Internal Volume	1,040 mL	1,030 mL	540 mL
Material	Aluminum 7075 T6	Aluminum 7075 T6	Aluminum 7075 T6
Maximum Pressure	23 bar	23 bar	160 bar

4.3. Ground Segment

MORSE will utilize NASA's Near-Earth Network ground stations for communication with the Earth. Four ground stations within the network are selected (Table 22). Each pair of closest ground stations are located within 120⁰ in longitude from each other, allowing continuous temporal coverage of the Moon. The antenna size, supported band, and transmitting EIRP are considered, as they are required to be compatible with the MORSE satellites. The communication relay is designed to operate in S-band, requires a high EIRP to transmit uplink from the Earth to the Moon, and a large-sized antenna to amplify the low-power signal from the Moon. The selected four ground stations are able to fulfil these requirements and are positioned to provide continuous temporal coverage.

Table 22: Specifications of Near-Earth Network Ground Stations for MORSE

	KSAT Singapore	South Point, Hawaii	Santiago, Chile	Hartebeesthoek, South Africa
Location	1.3962ºN, 103.8343ºE	19.0140ºN, 155.6633ºW	33.1511ºS, 70.6664ºW	25.8870ºS, 27.7120ºE
Available Assets	9.1m antenna	13m antennas (x2)	9m, 12m, 13m antennas	10m, 12m antennas
Supported Bands	S-band uplink, S/X-band downlink	S/X-band uplink, S/X-band downlink	S-band uplink, S-band downlink	S-band uplink, S/X-band downlink
EIRP (highest for S-band, dBW)	59	78	75	69
G/T (highest for S-band, dB/K)	20.5	23.5	25.7	22.4

4.4. Operational Process

4.4.1 Operational Modes

4.4.1.1 Launch Mode

During launch and translunar injection, whilst the spacecraft are still connected to the launch vehicle, all power and TT&C functions are provided by the launch vehicle, and only the onboard computer and the atomic clock are powered.

4.4.1.2 Detumbling Mode

Once separation from the upper stage occurs, the spacecraft will enter the Detumbling Mode. Using power from the fully charged battery, the onboard computer will turn on the ADCS sensors and reaction wheels to acquire and stabilize the spacecraft's attitude. The Earth-link transceiver and antenna will be activated and start transmitting tracking signals and telemetry to ground stations. Solar array panels will be deployed, rotating towards the sun using their sun tracking mechanism to start generating power.

4.4.1.3 Safe Mode

Once every essential subsystem for the cruise phase is operational, the spacecraft will enter Safe Mode for the rest of the trip to the Moon, in which all systems will be on standby.

4.4.1.4 Telemetry and Tracking Mode

Occasionally the spacecraft will enter Telemetry and Tracking Mode by switching on the Earth-link transmitter to send tracking signals and telemetry to ground stations within LoS.

4.4.1.5 Propulsion Mode

When the spacecraft arrive at the perilune, they will enter Propulsion Mode. They will use the chemical thrusters to perform the LOI maneuver to enter orbit around the Moon. In this mode, the transmitter will send tracking signal and telemetry to ground stations in real time for monitoring the thrusters' performance. After entering the mission orbit around the Moon, two of the spacecrafts will conduct phasing maneuvers to achieve equal spacing of 120º apart in terms of mean anomaly in

the orbit. The orbital phasing maneuver will take 83.5 hours to complete.

4.4.1.6 Operational Modes in the Mission Orbit

Once the three spacecraft have been equally spaced in the mission orbit, they will begin in-orbit performance verification testing to ensure that the spacecraft performance fulfills the requirements. Once testing has been completed and fulfilled required performance, relay and positioning services will begin.

The verification testing will evaluate the performance of the communication relay service and positioning service. For communication relay testing, the spacecraft will enter Relay and Positioning Service mode to establish communication link with the selected ground stations, then with neighboring MORSE spacecraft in orbit, and finally with the user. Test signals will be relayed to the Earth to evaluate the performance. If the signal integrity and C/N ratio fulfils the requirement, the service can be opened to commercial users. For positioning testing, as positioning is a proof-of-concept service, it will require users to provide feedback. Positioning accuracies will be relayed to Earth for evaluation.

In the mission orbit, the spacecraft will switch among Safe, Telemetry and Tracking, Positioning Service, and Relay and Positioning Service modes. When a spacecraft does not have LoS with clients in the Lunar South Polar region, it will be in Safe Mode to reduce power consumption and occasionally switch to Telemetry and Tracking Mode for telemetry downlink, tracking, and atomic clock calibration. The orbit of the constellation allows at least two spacecraft to have LoS with the clients at a given moment. Depending on the number of clients, the distance to the clients, and the volume of data that needs to be relayed, the spacecraft with LoS will either operate in the Positioning Service Mode or the Relay and Positioning Service Mode. The former broadcasts the positioning signal, while the latter relays data between clients and ground stations in addition to broadcasting the positioning signal. Whenever the onboard computer detects an anomaly in the spacecraft's status, it will command the spacecraft to enter Safe Mode to conserve power while the anomaly can be checked and addressed by the mission control.
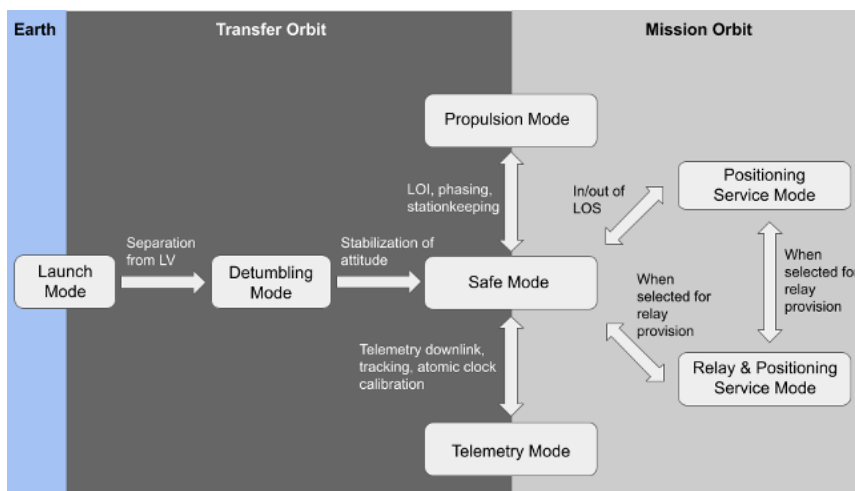

Figure 33: Overview of the operational modes

5. Concrete achievement methods, range and budget for manufacturing

Table 23: Hardware budget breakdown

Component	Quantity per Satellite	Total Estimated Price (USD)
Star Tracker	1	40,000
Sun Sensor	2	10,000
IMU	1	8,000
Reaction Wheel	4	28,000
Solar Array Panel	1	48,720
Solar Array Drive Assembly	1	400
Power Distribution System	1	58,080
Battery	11	76,560
Atomic Clock	1	1,000
Onboard Computer	1	5,280
Transceiver	2	43,200
Antenna	6	18,000
Main Thruster	1	100,000
Propellant Tank	3	15,000
Heater	10	760
Structure	1	19,000
Total per Satellite	N/A	502,000

6. Developing, manufacturing and launch schedule

The development and manufacturing schedule of MORSE is designed based on guidelines published by the NASA CubeSat Launch Initiative [19]. The development and manufacturing process is expected to start in November 2021 and take 24 months until launch. The large size and non-standard design of MORSE's satellite structure and the need to build three identical satellites makes this project long in comparison to many CubeSat projects. Due to the use of a dedicated launch vehicle and incompatibility with standard CubeSat dispensers, the time needed for launch vehicle integration and processing at the launch site is 40 days. This is based on the H-IIA User's Manual [20]. Launch is expected to take place on November 1, 2023. Figure 34 shows the planned time frame for each phase of the development and manufacturing process.
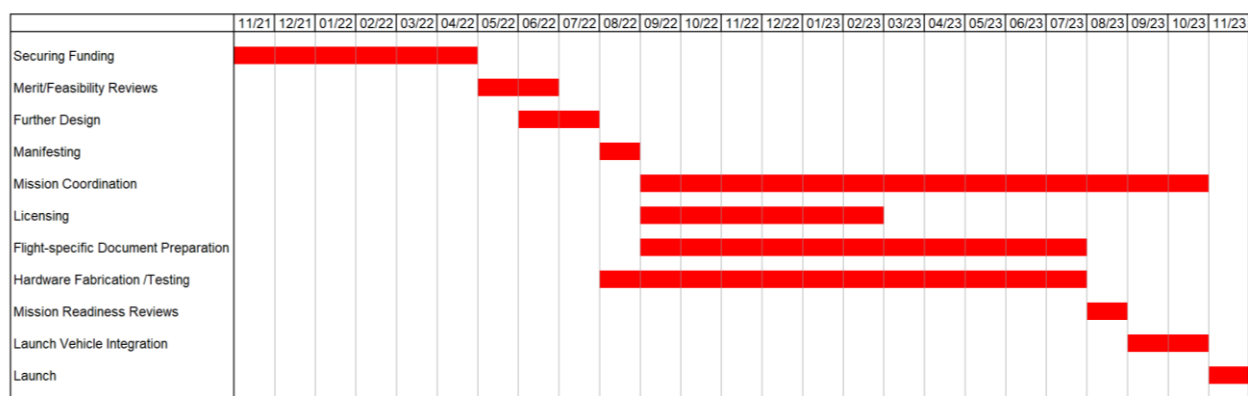
Figure 34: Development and manufacturing schedule of MORSE.

7. Conclusion

As the exploration of the Lunar South Pole increases over this decade, MORSE will provide a near-continuous communication relay and positioning service to the region from 2023 to 2028 using a constellation of three microsatellites. These services are expected to allow Lunar landers and rovers to reach more interesting places without being constrained by the availability of LoS and illumination. Entities with fewer resources will also be able to more easily take part in exploring the Lunar South Pole. Moreover, MORSE will serve as a pathfinder for a Lunar communications network and LNSS constellation that will continue supporting Lunar exploration beyond 2028 with more capable coverage and hardware. MORSE and its successors will facilitate the exploration and development of the Moon, which will not only generate new scientific knowledge about our Solar System but also serve as a stepping stone for humanity to become an interplanetary civilization.

8. References

[1]   H. Sasaki, "JAXA's Lunar Exploration Activities," in *62nd Session of COPUOS*, Vienna, 2019.

[2]   TASS, "China and Russia to launch 6 Lunar missions in 2021-2025 to build international Moon base," 17 June 2021. [Online]. Available: https://tass.com/science/1303403. [Accessed 3 November 2021].

[3]   L. Xu, Z. Pei, Y. Zou and C. Wang, "China's Lunar and Deep Space Exploration Program for the Next Decade (2020–2030)," *Chinese Journal of Space Science,* vol. 40, no. 5, pp. 615-617, 2020.

[4]   ispace, "Project," ispace, [Online]. Available: https://ispace-inc.com/project/. [Accessed 3 November 2021].

[5]   J. Flahaut, J. Carpenter, J.-P. Williams, M. Anand, I. Crawford, W. van Westrenen, E. Furi, L. Xiao and S. Zhao, "Regions of interest (ROI) for future exploration missions to the Lunar South Pole," *Planetary and Space Science,* vol. 180, p. 104750, 2020.

[6]   A. Gawronska, N. Barrett, S. Boazman, C. Gilmour, S. Halim, Harish, K. McCanaan, A. Satyakumar, J. Shah, H. Meyer and D. Kring, "Geologic context and potential EVA targets at the Lunar south pole," *Advances in Space Research,* vol. 66, no. 6, pp. 1247-1264, 2020.

[7]   P. Glaser, F. Scholten, D. De Rosa, R. Marco Figuera, J. Oberst, E. Mazarico, G. Neumann and M. Robinson, "Illumination conditions at the Lunar south pole using high resolution Digital Terrain Models from LOLA," *Icarus,* vol. 243, pp. 78-90, 2014.

[8]   B. Vanoutryve, D. De Rosa, R. Fisackerly, B. Houdou, J. Carpenter, C. Philippe, A. Pradier, A. Jojaghaian, S. Espinasse and B. Gardini, *An analysis of illumination and communication conditions near Lunar south pole based on Kaguya Data,* 2010.

[9]   B. Jolliff, N. Petro, D. Moriarty, R. Watkins, J. I. Head and R. Potter, "Sample Return from the Moon's South Pole-Aitken Basin," *Bulletin of the American Astronomical Society,* vol. 53, no. 4, p. 290, 2021.

[10]   T. Tanaka, T. Ebinuma and S. Nakasuka, "Dual-Satellite Lunar Global Navigation System Using Multi-Epoch Double-Differenced Pseudorange Observations," *Aerospace,* vol. 7, no. 9, p. 122, 2020.

[11]   L. Zhang, L. Xiong, J. Sun, S. Gao, X. Wang and A. Zhang, "Technical characteristics of the relay communication satellite "Queqiao" for Chang'e-4 Lunar farside exploration mission," *SCIENTIA SINICA Technologica,* vol. 49, no. 2, pp. 138-146, 2019.

[12]   T. A. Ely, "Stable Constellations of Frozen Elliptical Inclined Lunar Orbits," *Journal of the Astronautical Sciences,* vol. 53, no. 3, pp. 301-316, 2005.

[13]   M. Kaczmarzyk, M. Gawronski and G. Piatkowski, "Global database of direct solar radiation at the Moon's surface for Lunar engineering purposes," in *SOLINA 2018 - VII Conference SOLINA Sustainable Development: Architecture - Building Construction - Environmental Engineering and Protection Innovative Energy-Efficient Technologies - Utilization of Renewable Energy Sources*, Polańczyk, Poland, 2018.

[14]   B. Wie, H. Weiss and A. Arapostathis, "Quaternion feedback regulator for spacecraft eigenaxis rotation," *Journal of Guidance Control and Dynamics,* vol. 12, pp. 375-380, 1989.

[15]   F. Espenak, "NASA Goddard Space Flight Center Eclipse Web Site," NASA Goddard Space Flight Center, 27 August 2016. [Online]. Available: https://eclipse.gsfc.nasa.gov/. [Accessed 3 November 2021].

[16]   Tutorialspoint, "CDMA - Power Control," [Online]. Available: https://www.tutorialspoint.com/cdma/cdma_power_control.htm. [Accessed 3 November 2021].

[17]   E. Mahoney, "Disruption Tolerant Networking," 6 November 2020. [Online]. Available: https://www.nasa.gov/archive/content/dtn. [Accessed 3 November 2021].

[18]   ArianeGroup, "10N Bipropellant Thruster," [Online]. Available: https://www.space-propulsion.com/spacecraft-propulsion/bipropellant-thrusters/10-bipropellant-thrusters.html. [Accessed 3 November 2021].

[19]   NASA CubeSat Launch Initiative, CubeSat 101: Basic Concepts and Processes for First-Time CubeSat Developers, NASA CubeSat Launch Initiative, 2017.

[20]   Mitsubishi Heavy Industries, H-IIA User's Manual, Mitsubishi Heavy Industries, 2015.